Stationary Wavelet Processing and Data Imputing in Myoelectric Pattern Recognition on an Embedded System

An Approach to Continuous Myoelectric Control Systems Focused on Computational Efficiency

Master's thesis in Biomedical Engineering

ADAM NABER

Department of Electrical Engineering
CHALMERS UNIVERSITY OF TECHNOLOGY
Gothenburg, Sweden 2017

Master's thesis 2017

Stationary Wavelet Processing and Data Imputing in Myoelectric Pattern Recognition on an Embedded System

An Approach to Continuous Myoelectric Control Systems
Focused on Computational Efficiency

ADAM NABER

Department of Electrical Engineering
Division of Biomedical Engineering
Chalmers University of Technology
Gothenburg, Sweden 2017

Stationary Wavelet Processing and
Data Imputing in
Myoelectric Pattern Recognition
on an Embedded System
An Approach to Continuous Myoelectric Control Systems
Focused on Computational Efficiency
ADAM NABER

Supervisor: Max Ortiz-Catalan, Department of Electrical Engineering
Examiner: Bo Håkansson, Department of Electrical Engineering

Master's Thesis 2017
Department of Electrical Engineering
Division of Biomedical Engineering
Chalmers University of Technology
SE-412 96 Gothenburg
Telephone +46 31 772 1000

Gothenburg, Sweden 2017

Stationary Wavelet Processing and
Data Imputing in Myoelectric Pattern Recognition
on an Embedded System
An Approach to Continuous Myoelectric Control Systems
Focused on Computational Efficiency
ADAM NABER
Department of Electrical Engineering
Chalmers University of Technology

Abstract

Surface electromyography offers a low-cost, non-invasive method of predicting motor intention for prosthetic device control. Conventional active prostheses use individual muscle groups to trigger movement along one degree of freedom at a time, resulting in an effective, but slow and counter-intuitive control scheme. Pattern recognition-based approaches to decoding muscle signals allow for more advanced, intuitive control, but at the cost of robustness to in-band noise and sensor faults. Signal processing to increase the distinguishability of muscle signals is an active area of research, but there has been little investigation in the implementation of a real-time, portable system that is robust against common noise sources.

The aim of this work is to review the recent advances in electromyography signal processing and to investigate the effectiveness of wavelet-based signal processing and mean missing data imputing on the classification accuracy and controllability of myoelectric pattern recognition-based upper-limb prosthetic devices. The proposed algorithms were implemented on-board a standalone microprocessor to allow users of pattern recognition-based prosthetic devices to operate without being fixed to a PC.

Nine able-bodied subjects were instructed to perform a series of Motion Tests while generating motion artifacts and electrode disconnect events. Four channels of untargeted forearm electromyogram signals were recorded and used for motor intention prediction with and without the proposed routines active. The results for tests comparing wavelet-based transient artifact reduction and conventional filtering showed no statistically significant change. Results for comparing missing data imputation with standard processing also showed no statistically significant change.

Further tests were done using a recorded data set of 15 healthy subjects performing the same motion tests with artificially added pre-recorded motion artifacts and electrode disconnect events. In order to observe the effect of a higher number of episodes, further investigation was performed on a set of pre-recorded Motion Tests from 15 able-bodied subjects with artificially added noise and sensor faults. The tests with simulated interferences showed a statistically significant increase in classifier accuracy, specificity, and sensitivity for wavelet processing. Results also showed an increase in accuracy and specificity for data imputing, but at the cost of movement completion rate. These results suggest that the proposed routines can be implemented in real-time systems to improve prosthetic device controllability and that they are viable for use in further studies.

Keywords: electromyography, wavelet, stationary, imputing, pattern, recognition, signal, processing

Acknowledgments

This project would not have been possible without the guidance and support of Dr. Max Ortiz-Catalan and Enzo Mastinu, who were my lifelines throughout the duration of this work.
I would like to extend my thanks to everyone at the Chalmers Biomechatronics and Rehabilitation Laboratory and at Integrum A.B. for the technical support, equipment, and feedback that made this project a reality.
Finally, I would like to thank my partner, Jennifer, who made sure I managed to eat and sleep at regular intervals and supported me, even when I didn't come home until late at night.

Adam Naber, Gothenburg, June 2017

Contents

List of Figures

Acronyms

AFE Analog Front-End.
AR Autoregressive.

DoF Degree of Freedom.
DWT Discrete Wavelet Transform.

ECG Electrocardiogram.
EMG Electromyogram.

KNN K Nearest Neighbors.

LDA Linear Discriminant Analysis.
LOE Lead-Off Event.

MABS Mean Absolute Value.
MLP Multi Layer Perceptron.
MPR Myoelectric Pattern Recognition.
MSE Mean Squared Error.

sEMG Surface EMG.
SNR Signal-to-Noise Ration.
SSC Signed Slopt Change.
STFT Short Time Fourier Transform.
SVM Support Vector Machine.
SWT Stationary Wavelet Transform.

WL Waveform Length.
WT Wavelet Transform.

ZC Zero Crossing.

1
Introduction

1.1 Prosthetic Technology

Evidence of the use of prosthetic devices as both an assistive technology and for cosmetic replacement of missing limbs extends into antiquity. Only relatively recently, however, have commercial versions of these devices advanced beyond static objects or simple cable-driven systems. Rapid advancements in robotics technologies have begun to offer the real potential to truly replace missing functionality in disabled people.

For powered prosthetics, myoelectric signals from vestigial muscles are used as a control source due to their direct correlation to motor intention and ease of non-invasive detection [1]. There exists a significant discrepancy between the current mechanical prosthetic technology and the fidelity of the signal acquisition and control systems, resulting in limited controllability and frequent frustration from users [2]. One study performed in 2007 showed 39 % of upper-limb amputees with myoelectric prostheses do not use them regularly due to issues stemming primarily from low controllability and functionality [3], though the relationship between lost functionality and user requirements is complex and changes over time [4]. Artificial limb rejection rates have not been dropping in recent years, despite advances in signal processing technology, the addition of proportional speed control, and the adoption of functional hand grips by some manufacturers of upper-limb prosthetics [5, 6].

The vast majority of the consumer market for Myoelectric Controlled (MEC) devices uses threshold-based control schemes, referred to as Direct Control, where each independently controllable muscle group is linked to some movement. The of degrees of freedom (DoF) that the user can control simultaneously is limited by the number of electrode sites available on the vestigial limb. If only one site is available, referred to as Single Site control, two activity thresholds are used to code antagonist movements, e.g. opening and closing the hand depending on the strength of the contraction [7]. If two are available, called Dual Site control, the two muscles can code for antagonist movements on one DoF at a time, Fig. 1.1. These systems use either physical switches or co-contraction of antagonist muscles to cycle through the DoFs available in the prosthetic using a finite-state machine [8, 9]. While these systems are robust against noise, the slow switching and sequential nature of using a state machine makes control of the devices non-intuitive. High-level amputations in particular suffer from this due to the number of DoFs the prosthetic has to replace [10].

Significant clinical research has been done on using pattern-recognition to predict

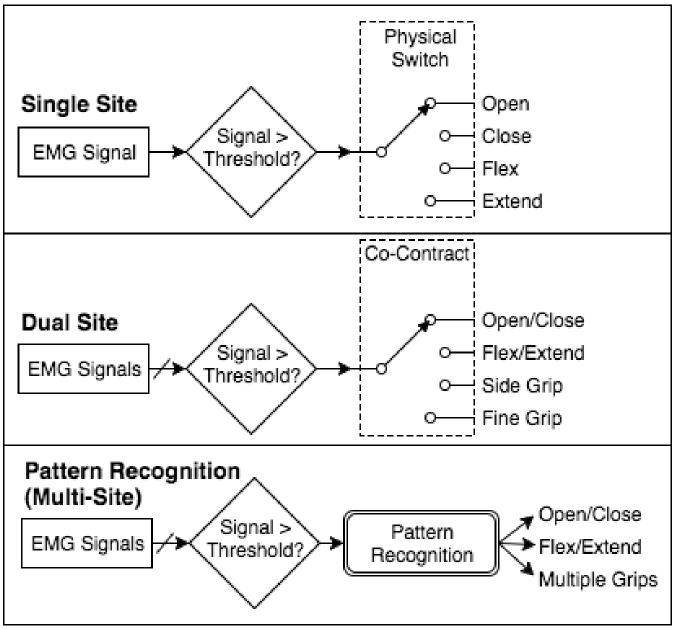

Figure 1.1: Block diagram illustrating common prosthetic control paradigms in commercial and clinical use.

motor intention using multi-channel surface Electromyogram (sEMG) recordings, negating the need for switching between different DoFs and potentially allowing for intuitive control, though the increase in functionality is offset by a large reduction in robustness [11]. This is an important point, as an incorrect movement of the prosthetic at any point has the potential to compromise an entire task [11]. Environmental noise, signal artifacts caused by electrode movement, and missing and corrupted signals due to loose electrode-skin contact are some of the most significant factors affecting sEMG signal integrity, especially for pattern-recognition based systems. Any systems that reduce the impact of these noise sources can have a significant positive affect on the controllability and robustness of clinical prosthetics [12].

1.2 Scope and Aim

The goal of this work is to investigate the implementation of signal processing and machine learning algorithms in an embedded prosthetic controller. The main tasks are listed as follows:

- analysis and summary of state-of-art technologies in the field
- implement at least one signal processing and one machine learning algorithm in the embedded controller
- implement wavelet-based signal denoising and artifact reduction
- implement sensor fault detection and data imputation
- evaluate the improvement in functionality and potential sources of errors

Included in this work is a scientific article containing the results and analysis for the proposed tests and routines.

1.3 Limitations

This thesis will not be concerned on the development of the hardware itself, but in the embedded software. As such, the ecological and ethical considerations of the project will not be covered in detail. Ethical approval for this work was previous obtained from the Regional Ethical Committee in Gothenburg, Sweden.

2
Background

Intuitive control is currently one of the main limitations for an upper-limb prosthetics in offering functional restoration of missing limbs [13]. Work done at Chalmers University of Technology, Sahlgrenska University Hospital and Integrum AB, has produced technology to interface an artificial limb to the patient's bone, nerves, and muscles. Analog and digital electronics have been combined to acquire and process bioelectric signals, decode motor intention, and restore sensory feedback. Several signal processing and machine learning algorithms have been developed for this application, however these have been mostly tested using personal computers instead of actual prosthetic devices [14]. Implementation of these algorithms in the prosthetic devices has the potential to improve the functionality of the devices, and thus the quality of life for the people that use them.

The end goal of any myoelectric pattern-recognition (MPR) system is to decode motor intention based on EMG signal characteristics. It is up to the signal preprocessing system to maximize the distinguishability of these features with respect to the available movement set. Historically, this has been limited to using conventional filters to attenuate signal frequency bands that are dominated by noise [15]. In recent years, more advanced techniques have been applied to the process aimed at decreasing the effect of noise on all signal bands [16]. One of these techniques, namely wavelet denoising, has shown considerable promise in increasing the Signal-to-Noise Ratio (SNR) of biological signals, and potentially the prediction accuracy of MPR systems [17, 18].

The current literature, to the authors' knowledge, is very limited on the use of wavelet-based signal processing for real-time signal reconstruction. Much of the research is focused on using subsets of the wavelet coefficients in pattern recognition directly [19, 20, 21, 22]. Some work has been done using wavelet-based processing for spike-sorting algorithms, but such a process typically requires high-density EMG or targeted muscle reinnervation [23]. The literature that does exist for generic pattern-recognition based approaches [18, 17] offers evidence on the possibilities of this processing paradigm, but does not explore the possibility of having the algorithms running with low latency on the prosthetic devices themselves.

2.1 Electromyogram

Electromyographic (EMG) signals are some of the most well understood and easily recorded bioelectric signals in the human body. Their direct correlation to muscle contractions and the availability of non-invasive recording mechanisms have made them the main focus of study for modern prosthetic control systems [1]. Despite this, finding an optimal strategy for interpreting the signals remains an open question, in no small part due to the noisy nature and large variability of biological systems in general.

2.1.1 Physiological Mechanism

Surface EMG signals are a chaotic summation of action potentials generated by discharges of motor units corresponding with the intended movement plus noise [9]. The action potentials, and resulting muscle activations, contain a large range of frequency components, but the higher-frequency components are filtered out in sEMG recordings as they pass through the tissue and smear with other muscle signals, Fig. 2.1. The dominant energy of the signal that reaches the surface of the skin is band-limited to about 500 Hz, meaning a sampling rate of at least 1 kHz with a low-pass filter at 450-500 Hz is sufficient for signal reconstruction [15]. The resulting EMG signal is considered non-stationary and stochastic, but can generally be treated as locally stationary for isometric muscle contractions on time windows of up to 1500 ms [9, 24].

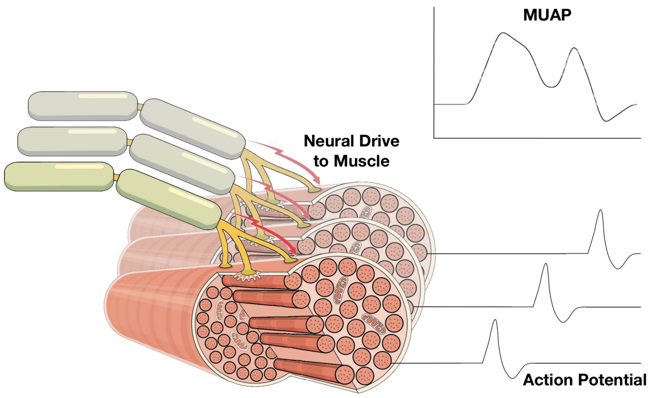

Figure 2.1: Generation of Motor Unit Action Potentials. Each muscle activation smears and merges with other nearby signals as it passes through tissue, making it difficult to identify individual activations [25].

2.1.2 Noise and Interference Sources

Noise inherent to the recording electronic equipment, power line noise, electrode lead-off events, motion artifacts, and biological signal instability are the dominant factors that degrade the SNR of sEMG signals [8]. Each noise source has different characteristics, with power line noise being the easiest to define and remove. The sEMG signal itself changes with respect to the changing distance between the skin surface and the signal source and the lengthening and shortening of muscle fibers during movements [11]. Changes in contraction strength result in a transient increase in higher frequency components, and can be seen in the time domain as an overall increase in the mean absolute value of the signal [7]. This property is exploited in some commercial prostheses for proportional control of either speed or force, but has the potential to cause misclassifications in MPR systems [26]. Muscle fatigue and electrode-skin impedance changes can also slowly alter the signal over time, requiring occasional adjustment of direct control or pattern recognition parameters. Transient changes in electrode impedance can be induced by contact artifacts, where a physical disturbance affects the interface and the underlying tissue. These artifacts are caused by temporary changes in capacitance, and are typically of much greater magnitude than the desired sEMG signals [12]. Artifacts caused by cable motion are common in many testing environments and have signal energy reaching up to around 50 Hz, making them difficult to remove without filtering out useful biological signals [27]. Dry socket prosthetics also suffer from the potential for electrode lead-off events (LOE), where a dry electrode becomes physically separated from the tissue as the shape of the stump changes. During these events, the affected channels contain no useful information, and have the potential to cause unintended movements based on the ambient electromagnetic noise they pick up.

Using more electrodes has the potential to offset some of these issues, especially in the case of transient noise or LOEs, where the issue may only affect one channel, but this also increases the complexity of the system and is only useful if there are enough active muscle sites on the vestigial limb [15]. The burden of detecting and compensating for these noise sources then falls to signal processing. Ideally, an algorithm to address the noise would increase the SNR while minimizing the distortion caused by signal manipulation [19].

2.2 Signal Processing

The aforementioned noise sources add a great deal of stochasticity to sEMG signals that must be reduced or, ideally, removed. Exactly how to achieve this remains an open question, but there has been investigation into a number of methods.

2.2.1 Conventional Filtering

The term *conventional filter* is used in this work to describe linear, time-invariant filters. They use a series of coefficients to describe a system with a response that reduces the amplitude of frequency bands in a given signal while minimizing distortion in the remainder. These are useful for anti-aliasing and to attenuate undesirable signals when their frequency bands do not overlap with the useful signals, called out-of-band noise.

High-pass filters with cutoff frequencies between 5 and 20 Hz are typical for sEMG applications, as very little signal below that range reaches the surface of the skin [15]. Notch filters can be used in certain circumstances to remove noise from small frequency bands inside the desired signal range, like in the case of 50 or 60 Hz power line filtering, at the expense of some signal distortion. While these filters are useful in removing certain unwanted characteristics of sEMG signals, they are by definition inflexible to time-varying changes in signal and noise sources and most forms of in-band noise.

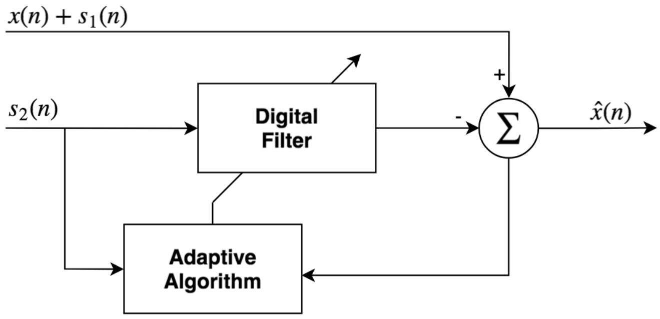

Figure 2.2: Block diagram of adaptive, noise canceling filter with signal source, $x(n)$, signal noise, $x_1(n)$, reference noise signal, $s_2(n)$, and filtered output, $\hat{x}(n)$.

2.2.2 Adaptive Filtering

Adaptive filters operate in a similar fashion as conventional filters with the exception that the coefficients are continuously updated to reduce some given error metric. They are of particular interest when an estimation of the noise is available, like in the case of power-line interference or when removing interfering electrocardiogram (ECG) signals from sEMG recordings [28]. Electrocardiogram signals are not typically an issue in standard upper limb prosthetics, but becomes a significant source of interference with patients who have undergone targeted muscle reinnervation (TMR), where the new muscle signals are recorded from the chest area [29]. Adaptive processing in the removal of ECG signals from EMG recordings is a well-researched field, and has been shown to be effective when working with TMR patients [29], respiratory EMG signals [30], and back muscle signals [31, 32]. The basic idea behind adaptive filtering is to iteratively update the filter coefficients by following the gradient of the signal error with respect to the coefficients, Fig. 2.2.
For the purpose of decoding upper limb sEMG motor intention, adaptive filtering by itself does not add significant value to the signal processing framework. Power line noise can be removed using less computationally demanding methods, ECG signals are only an issue with TMR patients, and since many of the noise sources cannot be recorded independently of the sEMG signal (i.e. cable and electrode motion artifacts and interfering biological signals), the noise reference required for adaptive filtering is typically unavailable.

2.2.3 Time-Scale Processing

The complex, time varying nature of sEMG signals and the noise they come with indicate a need for some statistical analysis that offers resolution in both the frequency and time domain in addition to conventional filtering.

2.2.3.1 Short-Time Fourier Transform

The Fourier transform, where a time-domain signal is projected onto the frequency domain, can be applied to arbitrarily small time windows. Using this property to analyze the frequency components of discrete time windows of a given signal is referred to as the Short-Time Fourier Transform (STFT), and adds temporal localization to the resulting coefficients. The time-domain resolution of this transform is inversely proportional to the size of the window and, in the case of discretely sampled signals, the frequency resolution is directly proportional to it. Using overlapping time windows for analysis increases the analytic power on larger time windows. As the ratio of window overlap to window size increases, though, it increases the computational complexity with a very limited effect in its ability to describe rapid fluctuations in the original signal [33]. Using highly-overlapping time windows to increase temporal resolution requires the system to maintain and analyze a large number of windows. Shrinking the window length reduces the memory and computational footprint, but also reduces the frequency resolution and increases the affect of windowing artifacts. A special case of this, called the sliding discrete Fourier transform, is a computationally efficient means of continuously separating time-domain signals into a small number of frequency bins. To the authors' knowledge, this technique remains entirely unexplored in processing EMG signals. The Wavelet Transform (WT) has been gaining popularity in overcoming the limitations inherent to STFT-based techniques, and is explored further in this work.

2.2.3.2 Discrete Wavelet Transform

The basic idea behind the Discrete Wavelet Transform (DWT) is to split a signal into compactly-represented time-domain signals along different frequency bands, allowing for the simultaneous analysis of spectral and time-domain properties of a signal. This is done by filtering the signal with a pair of quadrature mirror filters, whose magnitude responses are symmetric about $\pi/2$, and decimating the results, Fig. 2.3. The filters themselves are derived from an affine transformation of a prototype, or *mother*, wavelet. Based on the internal and mutual orthogonality properties of quadrature mirror filters, the resulting mapping is an orthogonal transformation, making it mathematically straight-forward to perform the inverse operation and allowing for the theoretically perfect reconstruction of the original signal. A rigorous proof and more detailed explanation can be found in [34].

The mapped values are referred to as the detail (high-pass) and approximation (low-pass) coefficients of the transform. The approximation coefficients can be fed into the algorithm again to provide the next level transform until either the desired level is reached or until there is only one approximation coefficient remaining. The detail and approximation coefficients represent the upper and lower half of the remaining frequency band, respectively, meaning a signal sampled at 1000 Hz would be split into detail coefficients that represent the 250-500 Hz frequency band and approximation coefficients that represent the 0-250 Hz frequency band on the first level of the transform.

The DWT has gained significant popularity in recent years for analyzing and reducing noise in biological signals, but research has been limited to offline analysis on large time windows, leaving its efficacy in real-time applications in question [24, 35, 28]. One of the main drawbacks to the DWT is that it contains limited localization information at increased levels of the transform. A given position along one level of the transform does not necessarily correspond to any integer position on another level, making it difficult to perform multi-resolution analysis, Fig. 2.4.

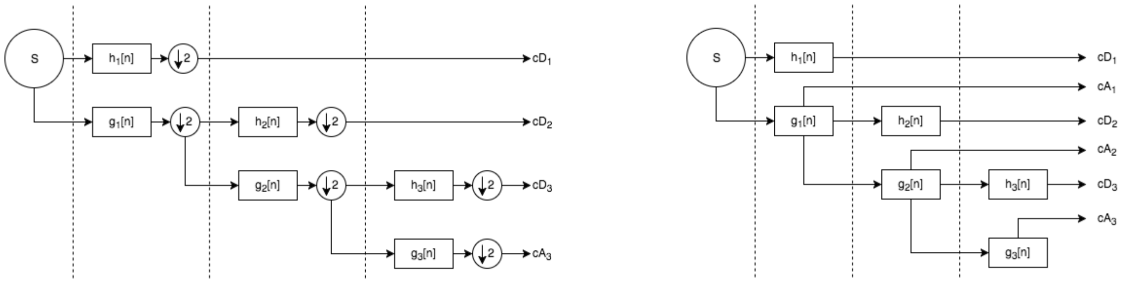

Figure 2.3: Block diagrams for the Discrete (left) and Stationary (right) Wavelet Transforms. The Stationary Wavelet Transform outputs remain undecimated, and the filters for each level are upsampled versions of the previous level filters.

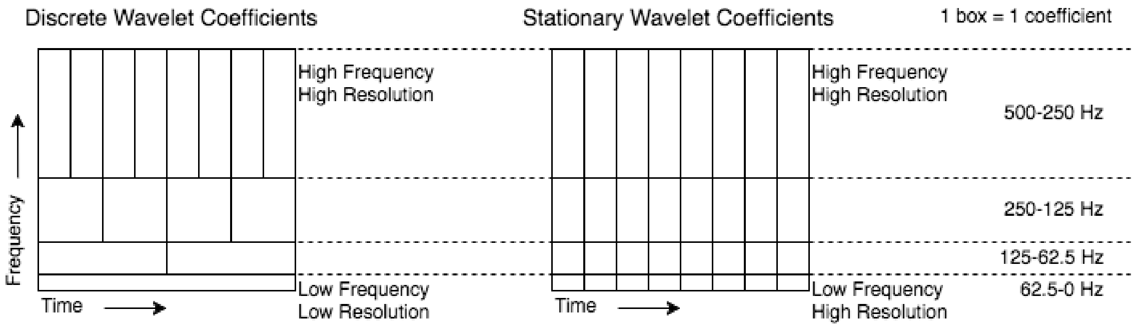

Figure 2.4: Fourth level discrete (left) and stationary (right) wavelet transform coefficient mappings

This restriction can be addressed by calculating multiple DWTs with different starting points for the decimation operator (referred to as an ε-decimated DWT), or by performing the Stationary Wavelet Transform.

2.2.3.3 Stationary Wavelet Transform

The Stationary Wavelet Transform (SWT) is similar, in principle, to the DWT with the exception that it forms an over-determined representation of the original data that represents all possible ε-decimated DWT. It does this by, instead of decimating the coefficients, upsampling the high- and low-pass filters at each stage, Fig. 2.3. This affords a one-to-one correlation between each position along all levels of the transform, shown in Fig. 2.4.

2.2.4 Fault Tolerance and Data Imputing

Accurate amplifier operation relies on having an input impedance significantly higher than that of the target circuit. As the target circuit impedance grows, the signal reaching the amplifier becomes attenuated, resulting in an increase affect of noise sources on the signal features. This is especially true for sEMG signals, which require high amplification to be effectively measured. Ag/AgCl gel electrodes fixed to the arm typically have an impedance ranging from between 50-1000 kΩ, depending on placement and skin preparation [36], and dry electrodes have an even greater

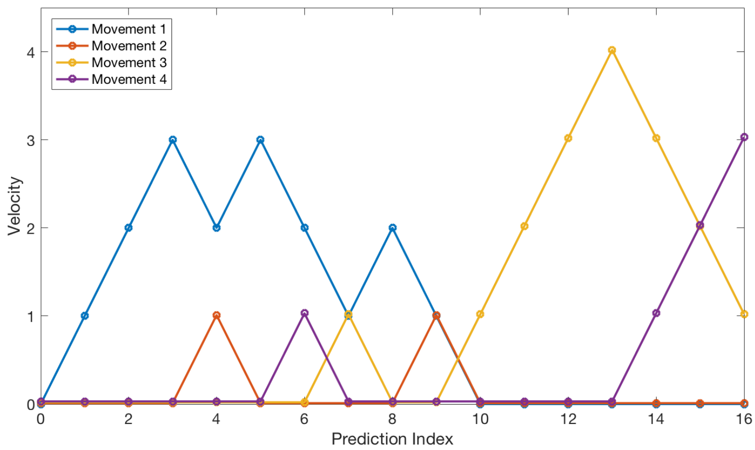

Figure 2.5: Example of a linear ramp function. The lines represent each possible classification other than rest and the y-axis represents the movement velocity of each class at each prediction index.

variance, so sEMG amplifiers typically have an input impedance on the order of hundreds of MΩs.

Existing classifiers that adapt to slow changes in signal characteristics have limited usefulness in handling electrode lead-off events (LOE), where the electrode becomes physically separated from the skin, as the noise generated by them is characterized by the sudden and complete loss of EMG signal. One potential solution is to simply train the classifier with each combination of channels having lead-off noise, but this is very memory intensive depending on the number of features and channels, and is not appropriate for embedded applications.

Majority voting and ramp functions are popular post-processing methods of increasing the robustness of classifiers to signal transients [9, 37]. Majority voting takes a sliding window of predictions and outputs the classification with the highest occurrence within that window. The ramp function uses a count of recent previous classifications to determine the velocity of the predicted movement, allowing for proportional control [37]. While this does not completely eliminate spurious movements that would be removed by majority voting, it significantly reduces their effects, illustrated in Fig. 2.5. It is a bit more flexible than majority voting, as the rising and falling ramp functions can be specified to suit the data. The increase in robustness both these methods offer comes at the cost of additional delay, as they increase the amount of time between the first movement classification and full speed output activation. This makes the size of the post-processing windows and ramp function, if used, crucial factors for intuitive and responsive control.

It may not be necessary to stop classification or use a very robust classification method, depending on the amount of redundancy contained in the remaining sensor data [38]. Zhang *et al.* demonstrated that a Linear Discriminant Analysis classifier tolerant to electrode faults results in increased classification accuracy, suggesting that the loss of information during LOEs is a legitimate cause for concern [12]. Their implementation used a fast retraining algorithm for the classifier that compensated

for missing channels. While promising, it does not provide a generic solution applicable across different machine learning algorithms.
Pelckmans *et al.* [39] suggested using a probabilistic model of missing data for SVMs that approaches mean data-imputing in the case of a linear classifier [38]. While the research has not yet been applied to sEMG signals specifically, it offers a generic solution that is computationally efficient on linear classifiers and theoretically feasible on non-linear ones.

2.3 Feature Extraction

The data set required to train pattern recognition algorithms needs to be highly overdetermined, meaning there needs to be many more observations than dimensions in the feature space [40]. This makes it difficult to feed even a highly-processed sEMG signal directly into a classifier and expect anything useful in return. To accommodate for this, the time-domain signals are typically windowed and a small set of signal features are calculated on each window.

2.3.1 Data Windowing

The amount of information a given time window contains is directly proportional to its length, but so is the controller delay it imposes on the system. Taking a naïve approach to segmenting data leads to discrete time windows, where the data in each window is unique. A deeper analysis of the problem, however, suggests using windows with some overlap, Fig. 2.6. Doing this adds redundancy and robustness to the classification system and increases the throughput. Combining this with a ramp or majority voting scheme for prosthetic device control can significantly increase the robustness of a given classifier without affecting the response time.

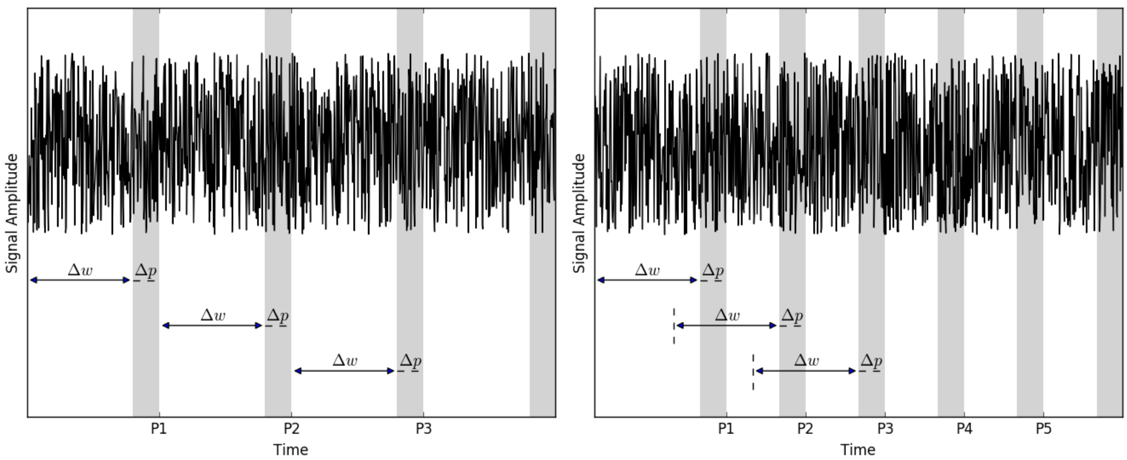

Figure 2.6: Examples of discrete (left) and overlapping (right) windowing methods. Grey areas represent the processing time, and each tick mark along the x-axis denotes a prediction. Δw denotes the window length, Δp denotes the processing time, and P_i denotes the i-th prediction. Note that overlapped windowing produces predictions with the greatest frequency.

For sEMG control systems, using smaller, overlapping windows for feature extraction is appropriate, as it reduces overall controller delay while maintaining a window large enough to contain useful information. Selecting a window size that allows for total data collection and processing time less than around 200-250 ms is recommended to prevent the device from feeling sluggish [41]. Farrell *et al.* showed that windows as small as 150 ms still perceptibly degrade the performance of prosthetic limbs, but their experiments dealt with dual-site direct control along one DoF, meaning they didn't incorporate the affects of misclassifications in their analysis [42]. Some research indicates controller delays of up to 400 ms are still considered responsive [15, 43], but given that the minimum time between distinct muscle contractions is closer to 200 ms, shorter time windows are typically chosen to prevent time windows from containing signals from more than one motion [15].

2.3.2 Signal Features

There are many signal features that can be used for classification, but time domain features typically outperform time-scale and frequency domain features on steady-state EMG signals and introduce less computational complexity [9].

2.3.2.1 Time Domain Features

The Time Domain (TD) feature set proposed by Hudgins *et al.* [43] contains some of the most commonly investigated features, due to their very low computational complexity and high descriptiveness of both time- and frequency-domain properties of sEMG signals [24, 19]. A relative comparison of TD features suggests the use of four features from this set [8, 44]: mean absolute value (MABS), zero crossings (ZC), waveform length (WL), and signed slope change (SSC), defined in Equations (2.1-2.4).

$$\mathrm{MABS} = \frac{1}{N}\sum_{i=1}^{N} |x_i| \tag{2.1}$$

$$\mathrm{ZC} = \sum_{i=1}^{N-1} \begin{cases} 1, & |x_i - x_{i+1}| \geq \mathrm{MABS} \\ 0, & \text{otherwise} \end{cases} \tag{2.2}$$

$$\mathrm{WL} = \sum_{i=1}^{N-1} |x_{i+1} - x_i| \tag{2.3}$$

$$\mathrm{SSC} = \sum_{i=1}^{N-1} \begin{cases} 1, & \mathrm{sgn}(x_i - x_{i-1}) \cdot \mathrm{sgn}(x_i - x_{i+1}) < 0 \\ 0, & \text{otherwise} \end{cases} \tag{2.4}$$

where $N \in \mathbb{N}$ is the window length in samples, $x_i \in \mathbb{R}$ is the sample at time index $i = 1, ..., N$.

2.3.2.2 Autoregressive Coefficients

Autoregressive (AR) model coefficients can be used as EMG signal features and have been shown to increase predictive power when used in addition to TD features [20].

AR models are useful in general for approximating linear, time-varying, stochastic systems. An p-th order AR system, denoted by $AR(p)$, relies on a set of linear coefficients, $\overrightarrow{a} \in \mathbb{R}^p$, and a white noise parameter, e, to estimate future values of a system using past data:

$$x_i = \sum_{k=1}^{p} a_i x_{k-i} + e_i, \qquad i = 1, ..., N, \tag{2.5}$$

where x_i denotes the recorded EMG signal. In the case of EMG feature extraction, the coefficients are used to describe the signal, rather than predict future values. AR(4) is commonly used in EMG signal processing, as it provides an acceptable trade-off between descriptive power and computational complexity [45, 24].

2.3.2.3 Other Metrics

Information metrics, like entropy, offer a non-linear feature space that improves the distinguishability of isometric contractions, but without special hardware, calculating these features is very computationally expensive [20]. A more comprehensive description of commonly used features in EMG signal classification can be found in [24].

2.4 Pattern Recognition

Pattern recognition systems, a subset of machine learning, recognize patterns in the structure of the input data to either perform a regression or classification. The systems used in this work are all supervised classification models, meaning they use training samples with known classes to minimize the predictive error. One of the advantages these systems have over direct control is that they are able to recognize muscle synergies, meaning that the muscle cross-talk that is detrimental to direct control schemes becomes useful information and increases predictive power of the classifier [20].
The processing and memory requirements of many pattern recognition systems limits the selection for real-time embedded applications to a small number of choices that have low memory footprints and simplify to solving matrix and vector operations, which modern digital signal processors are optimized for. Multi-Layer Perceptron (MLP), Support Vector Machine (SVM), and Linear Discriminant Analysis (LDA) all meet these constraints and demonstrate classification performance on par with more advanced algorithms in sEMG applications in previous research [8].

2.4.1 Support Vector Machine

The basic principle behind the support vector machine (SVM) is to find the hyperplane that best separates two classes in a feature space using the set of data points closest to the class boundary. Given a training data set $(\overrightarrow{x}_1, y_1), ..., (\overrightarrow{x}_N, y_N)$, where $\overrightarrow{x}_i$ is the i-th data point in the given feature space and $y_i \in \{-1, 1\}$, representing the class $\overrightarrow{x}_i$ belongs to, it finds the parameters $\overrightarrow{w}$ and b such that the hyperplane defined by:

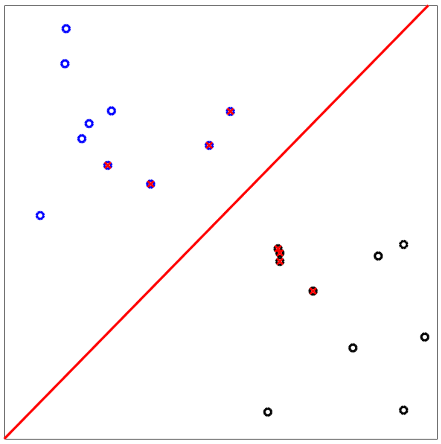

Figure 2.7: The maximum-margin linear hyperplane for a 2D, 2 class system. The samples on either side of the margin with the filled circles are called support vectors, as they determine the location of the hyperplane.

$$\overrightarrow{w} \cdot \overrightarrow{x} - b = 0 \tag{2.6}$$

maximally separates the nearest training data points between the two classes, Fig. 2.7. The resulting plane is referred to as the maximum-margin hyperplane. Predicting the class, y_p, of a new data point, $\overrightarrow{x}_p$ is defined by the following equation:

$$y_p = \mathrm{sgn}(\overrightarrow{w} \cdot \overrightarrow{x}_p - b) \tag{2.7}$$

This system can been extended to support nonlinear classification with the use of a learned, nonlinear kernel function replacing the the hyperplane [46]. Regardless of the hyperplane function, the SVM is by definition a binary classification system. Multi-class support for the algorithm can be achieved by a few methods, the simplest being a *one-vs.-all* approach. Bitzer and Van der Smagt demonstrated this to be a reliable system in their work on decoding sEMG signals [47, 20]. For a k-class system, k independent SVM classifiers are trained to distinguish each class from the rest and are stacked, resulting in a matrix $W \in \mathbb{R}^{k \times q}$ where q is the number of features and a vector $\overrightarrow{b} \in \mathbb{R}^k$. Classifications are performed by finding the maximum resulting value in each of the SVMs, or as a matrix operation:

$$y_p = \max(W\overrightarrow{x}_p - \overrightarrow{b}) \tag{2.8}$$

2.4.2 Linear Discriminate Analysis

Linear discriminate analysis (LDA) approaches feature classification by creating a decision boundary that separates the mean values of data in each class, rather than the closest points to the boundary, weighted by the within-class covariance. The mean feature values, μ_0 and μ_1, and covariances, Σ_0 and Σ_1, are calculated for two classes to form the parameters:

$$\vec{w} = \Sigma_1^{-1}\vec{\mu}_1 - \Sigma_0^{-1}\vec{\mu}_0 \tag{2.9a}$$

$$c = \frac{1}{2}\vec{\mu}_1^T\Sigma_1^{-1}\vec{\mu}_1 - \vec{\mu}_0^T\Sigma_0^{-1}\vec{\mu}_0 \tag{2.9b}$$

where $\vec{w}$ represents the vector normal to the decision boundary separating the class-specific means and c represents the location along that vector where the boundary occurs. Classification is performed by thresholding along the projection formed by the sample point $\vec{x}$ along $\vec{w}$:

$$y_p = \mathrm{sgn}(\vec{w} \cdot \vec{x} - c) \tag{2.10}$$

Like the SVM classifier, LDA is a binary classification algorithm. The same system described above can be used to effectively train a multi-class LDA system.

2.4.3 Multi-Layer Perceptron

Multi-Layer perceptron neural networks are a popular class of non-linear machine learning algorithms. They are intended to roughly model the neural interactions using layers of units, called perceptrons, to form novel ways of interpreting data. MLP networks form a fully connected acyclic directed graph, meaning all perceptrons in each layer take in a weighted sum from all outputs from the previous layer before feeding it into a non-linear activation function, Fig. 2.8. The number of perceptrons in each layer, the number of layers, and the activation functions each layer uses are all independent, and are tunable to fit the structure and complexity of the data. The activation functions used in neural networks vary considerably, but monotonic, continuously differentiable functions, like the hyperbolic tangent and the logistic function, are popular for MLP networks:

$$\phi(x) = \tanh(x) \quad \text{and} \quad \phi(x) = (1 + e^{-x})^{-1}, \quad x \in \mathbb{R}. \tag{2.11}$$

MLP networks can be trained by iteratively adjusting the perceptron weights to minimize error of the system. This is typically done starting at the output perceptrons and working backwards, called backpropagation. The activity of a single perceptron in layer j, $x_{j,k}$, subject to an activation function, $\phi(x)$, can be described as follows:

$$x_{j,k} = \phi\left(\sum_{i=1}^{I_j} w_{j,k,i}x_{j-1,i} + b_j\right) \tag{2.12}$$

$$= \phi(v_{j,k}), \tag{2.13}$$

where I_j is the number of neurons in layer $j = 1, ..., J$ and J is the total number of layers in the neural network. Bias terms, b_j are added to prevent the decision boundary from being fixed at the origin. The neural network classifier is then trained by

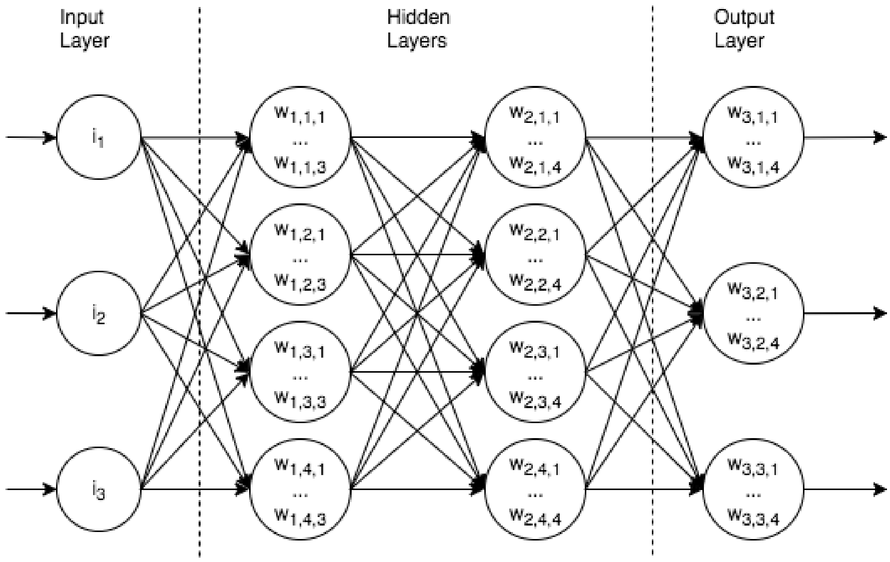

Figure 2.8: MLP Neural Network block diagram. The input layer consists of the features fed into the classifier. Each hidden layer feeds a weighted sum of all perceptrons in the previous layer into an activation function that feeds into the next layer.

minimizing a cross-entropy function with a process called back-propagation. Back-propagation calculates the gradient of the cross-entropy function with respect to each weight on each iteration. The training process does not guarantee the global minimum or even convergence, depending on the learning rate, but finding an analytic solution to a given MLP network becomes extremely difficult as the complexity of the network grows [48].

2.4.4 Other Systems

While the machine learning approaches listed above are popular choices for EMG applications, they are not without drawbacks. The assumption of linearly separable data distributions that linear classifiers rely on are not always sufficient to describe complex systems.. Nonlinear systems, like the MLP network, are susceptible to overfitting and often have no way of guaranteeing a globally optimal solution [20]. Other methods exist that overcome these limitations, with drawbacks of their own, some of which are detailed below.

2.4.4.1 K-Nearest Neighbors

The K-Nearest Neighbors (KNN) classification algorithm is possibly the most intuitive machine learning system. The naïve approach compares the Euclidean distance between each item in the training set and the test sample. The k nearest training points are then used in a majority vote to determine which class the new point is most similar to. One of the primary drawbacks to KNN classifiers that limits their applicability in real-time and resource constrained environments is the computational and memory complexity involved in storing and calculating metrics on the

entire training set.
Using hyperplanes to partition the feature space, called Voronoi tessellation, and various clustering and compression algorithms have been proposed to reduce this overhead, but their applicability for myoelectric control has yet to be investigated [49, 50, 51]. Alternative distance metrics, like the Mahalanobis distance, Manhattan distance, and Chebyshev distance, are frequently used in KNN applications to reduce computational complexity or better describe the feature space [50], but to the authors' knowledge, have not been extensively investigated in EMG applications.

2.4.4.2 Fuzzy Networks

Fuzzy logic systems are robust against incomplete and contradictory data, which are often present in EMG data and other biological signals. They also have the capability to incorporate information on physiologically compatible movements and other *a priori* knowledge of common tasks directly into their decision making algorithm [19].
Fuzzy classifiers operate by mapping numerical variables into linguistic values that describe a continuous range that feature may occupy, like *high*, *medium*, and *low*. The equation that determines the degree to which a value falls in each of the ranges is referred to as the *input membership function*. To fully describe a decision rule set involving n features and M linguistic values, M^n rules are necessary. These rules amount to a lookup table in computational terms, making them fast and efficient to execute, but require increasing amounts of often counter-intuitive manual configuration as the feature space grows.
Optimization of the values described by the linguistic variables and generating the lookup table for classification can be automated by applying heuristic clustering and neural network systems to fuzzy classifiers, respectively. The most common type of clustering used for fuzzy classifiers is fuzzy c-means optimization [52]. Given a number of clusters, c, it iteratively optimizes the following objective function to find the optimal cluster locations, $\overrightarrow{v}$, with respect to the matrix membership function, U:

$$J(U, \overrightarrow{v}) = \sum_{k=1}^{n} \sum_{i=1}^{c} u_{i,k} d_{i,k}^2 \tag{2.14}$$

where $d_{i,k}$ indicates the Euclidean distance between data point k and the i-th cluster center, and $u_{i,k}$ represents the membership function applied to the same data point and cluster center. After the cluster centers have been generated, back-propagation (described in Multi-Layer Perceptrons) can be applied to optimize the output decision parameters to determine which input membership ranges correspond to which classifier outputs. Such systems are referred to as neuro-fuzzy classifiers, and have been demonstrated to show an accuracy equivalent to Bayes classifiers and nonlinear discriminant functions [9].
Depending on how the output function is set up, fuzzy classifiers have the ability to produce either *crisp* or *fuzzy* classifications, illustrated in Fig. 2.9. Using fuzzy classifications offers an opportunity for simultaneous, proportional control in MEG prostheses, but investigation into such a system has been largely left to speculation.

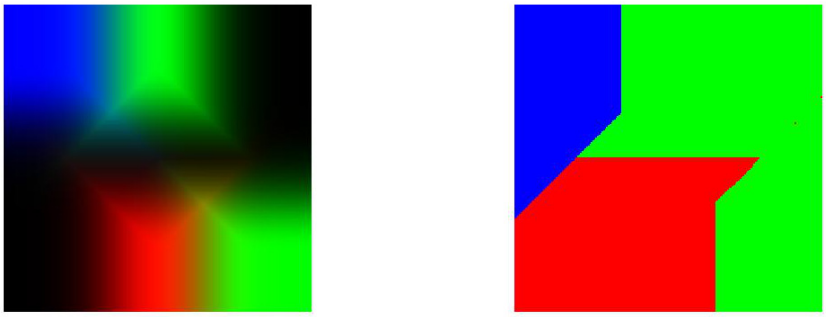

Figure 2.9: Classification regions formed by three classes in a two dimensional feature space with fuzzy (left) and crisp (right) classification regions. The dark areas correspond to regions where the output is low for all classifications and indicates that the description of the feature space is incomplete.

3
Methods

This section contains an overview of the hardware and software used as well as the methods and results for the selection of optimal wavelet processing parameters. It serves as an expanded version of the methods listed in the attached article in appendix A. In addition to the items listed in this section, an efficient implementation of a generic MLP classifier was written for the system, but was unused in this research due to its poor performance for this application shown in the preliminary analysis.

3.1 Microcontroller Setup

Existing firmware that included routines for signal acquisition, conventional filtering, feature extraction, and LDA and linear SVM pattern recognition algorithms was used in this experiment and modified where appropriate. The base firmware was provided by Integrum AB working in conjunction with the Chalmers Biomechatronics and Rehabilitation Laboratory.

3.1.1 Stationary Wavelet Transform

No microcontroller-compatible implementations of the stationary wavelet transform or its inverse was found, so one was written in C and optimized for the Tiva C-Series TM4C123G microcontroller. The implementation leveraged the publicly available Cortex Microcontroller Software Interface Standard libraries [53].

3.1.2 Sensor Fault Detection

Electrode disconnect events create high impedance mismatch between the amplifier and the leads. To detect this, a 6 nA DC current source was fixed to both the positive and negative leads of each amplifier and the input impedance for each amplifier is set to 500 MΩ, shown in Fig. 3.1. During normal operation, the signal harmlessly dissipates through both the patient and the amplifier, but will saturate the amplifier input when either or both leads are disconnected from the patient. This saturation was addressed by applying hard thresholding to any signal outside the 30-70% maximum value range of the amplifier, corresponding to approximately ± 66 μV. Signals outside of this range were replaced with the mean value, which is 0 V for sEMG signals [15].

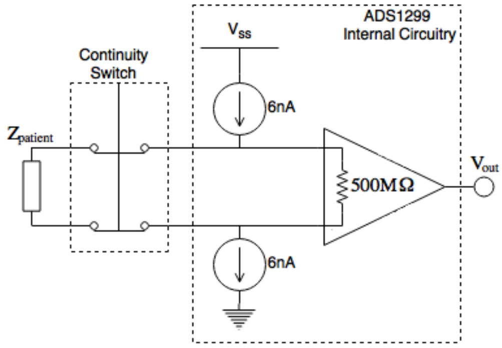

Figure 3.1: Equivalent circuit for detection and simulation of lead-off events in real-time.

3.1.3 Data Imputing

Mean data imputing for missing samples was chosen in this work due to its intuitive affect on the signal and its computational simplicity. More advanced methods do exist based on statistical analysis of previous data, applications of machine learning algorithms in the prediction of new data, and template matching. Each of these offer different advantages depending on the application at the cost of time and memory, and may be worth investigation into the processing of sEMG signals if the proposed approach is insufficient, but are out of the scope of the current work. An overview of many of these methods can be found in [38].

3.1.4 Wavelet-Based Denoising

The sEMG signal and noise sources both have stochastic, time-varying properties that overlap in the frequency domain, limiting the usefulness of conventional filtering to treating out-of-band signals and power-line noise [8]. Statistical analyses of sEMG signals in the time-scale domain can be used to dynamically shrink noise components in a window-based approach based on *a priori* knowledge of the signal and noise properties [54]. The frequency characteristics of sEMG signals depend on a number of factors, but the dominant frequency band viable for wavelet analysis is in the 125-250 Hz range [19], and components in the 250-500 Hz range are dominated by system noise [15]. In this case, the system noise is treated as a locally-stationary additive function based on the standard deviation of the first-level wavelet coefficients.

Algorithms to reduce system noise from wavelet coefficients were selected based on reviews in previous literature with an emphasis on computational simplicity [18, 54, 55, 56, 57, 58]. Hard, soft, semi-hyperbolic, adaptive, and non-negative shrinkage methods were investigated in this experiment, defined as:

$$\text{Hard}: \quad \hat{\gamma}_{j,i} = \begin{cases} \gamma_{j,i}, & |\gamma_{j,i}| > \lambda, \\ 0, & \text{otherwise}, \end{cases} \tag{3.1}$$

$$\text{Soft}: \quad \hat{\gamma}_{j,i} = \begin{cases} \gamma_{j,i} - \lambda, & |\gamma_{j,i}| > \lambda, \\ 0, & \text{otherwise}, \end{cases} \tag{3.2}$$

$$\text{Hyperbolic}: \quad \hat{\gamma}_{j,i} = \begin{cases} \text{sgn}(\gamma_{j,i})\sqrt{\gamma_{j,i}^2 - \lambda}, & |\gamma_{j,i}| > \lambda, \\ 0, & \text{otherwise}, \end{cases} \tag{3.3}$$

$$\text{Adaptive}: \quad \hat{\gamma}_{j,i} = \gamma_{j,i} - \lambda + \frac{2\lambda}{1 + \exp(2.1\gamma_{j,i}/\lambda)}, \tag{3.4}$$

$$\text{Non-Negative}: \quad \hat{\gamma}_{j,i} = \begin{cases} \gamma_{j,i} - \frac{\lambda^2}{\gamma_{j,i}}, & |\gamma_{j,i}| > \lambda, \\ 0, & \text{otherwise}, \end{cases} \tag{3.5}$$

where $\gamma_{j,i}$ denotes the original wavelet coefficient at level j at time index i and $\hat{\gamma}_{j,i}$ denotes the denoised wavelet coefficient the same index.
The Daubechies 4 tap mother wavelet was chosen as the mother wavelet due to its good performance in describing time and frequency components and its computational simplicity [17]. The noise threshold parameter, λ, for each routine was calculated using minimaxi threshold, intended to minimize the maximum mean squared error against an ideal procedure [59, 17]:

$$\lambda = \hat{\sigma}\left(0.3936 + 0.1829 \cdot \frac{\log(N)}{\log(2)}\right) \tag{3.6}$$

where $\hat{\sigma}$ is the standard deviation of the system signal noise wavelet coefficients and N is the window length in samples.
Zhou *et al.* [29] provided a comparison of wavelet-based hard thresholding against conventional filtering, adaptive filtering, and other processing techniques on the removal of corrupting ECG signals from EMG data. They found that wavelet-based denoising effectively removes the ECG artifacts with minimal corruption of the signal's mean amplitude, though this work did not include analysis on the affect of wavelet-based denoising on other signal features.

3.1.5 Wiener Wavelet Filtering

One of the documented effects of the WT is that it tends to concentrate the signal energy into a relatively small number of high-valued coefficients [60]. Wavelet-based denoising then reduces any sufficiently small coefficients (assumed to be noise) towards zero, reducing the signal subspace (the number of non-zero coefficients used to describe the signal). Combined with the fact that the WT provides rich spectral characteristics on both the desired signal and the noise, this process lends itself to Wiener filtering, expressed as $\tilde{\gamma}_{j,i}$ in:

$$\tilde{\gamma}_{j,i} = \frac{\gamma_{j,i} \cdot \hat{\gamma}_{j,i}^2}{\hat{\gamma}_{j,i}^2 + s(\hat{\gamma}_1)^2}, \tag{3.7}$$

where $s(\cdot)$ denotest the corrected sample standard deviation. This treats the desired signal and the noise as locally stationary systems, which is appropriate for sufficiently small windows, and provides a smoother system response than wavelet shrinkage alone. It should be noted that the Wiener filtering coefficients *can* be calculated on WT with a different transform level and mother wavelet selection than the original data, Fig. 3.2, but this flexibility was foregone in this implementation in lieu of better real-time performance.

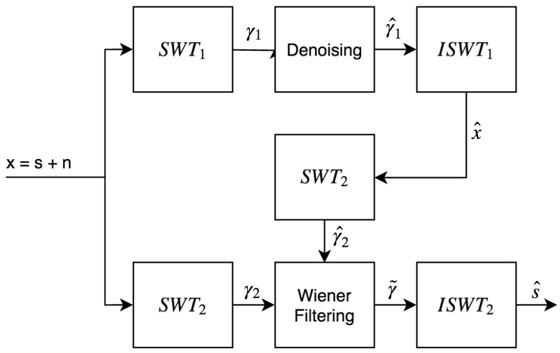

Figure 3.2: Block diagram for generic wavelet-based Wiener filtering. Note that the transforms for the Wiener coefficient estimation and for the signal filtering are separate, allowing for use of different wavelet parameters in wavelet shrinkage and Wiener filtering.

3.1.6 Artifact Reduction

Since most of the signal energy in motion artifacts of all types typically occurs at or below 20 Hz [16], a fourth-order wavelet transform can cleanly separate the signal bands without loss of information. In this implementation, it is assumed that any strong signal in the approximation coefficients of the transform (corresponding to the 31.25-0 Hz range) is a transient artifact. Hard thresholding is applied to each signal band in the following manner to remove the corrupted portions of the signal:

$$\mathrm{thr}_k = \mu_i(|\gamma_{\mathrm{dom}}|) + k \cdot s_i(\gamma_{\mathrm{dom}}) \tag{3.8}$$

$$\hat{\gamma}_{A,i} = \begin{cases} \gamma_{A,i}, & \text{if } |\gamma_{A,i}| < \mathrm{thr}_1, \\ 0, & \text{otherwise,} \end{cases} \tag{3.9}$$

$$\hat{\gamma}_{D,i} = \begin{cases} \gamma_{D,i}, & \text{if } |\gamma_{A,i}| < thr_1 \cup |\gamma_{D,i}| < \mathrm{thr}_0, \\ 0, & \text{otherwise,} \end{cases} \tag{3.10}$$

where $\gamma_{A,i}$ is the i-th wavelet approximation coefficient, $\gamma_{D,i}$ is the corresponding detail coefficient at decomposition level D, γ_{dom} is the wavelet decomposition level corresponding to the dominant frequency band, and $\mu(\cdot)$ is the mean function.
A strong transient artifact can have components that smear across the entire frequency spectrum, depending on how quickly the onset and offset of the artifact

occur. The proposed method of artifact reduction aims to remove only the corrupted portions of the signal from each of the frequency bands in the described manner. The effect of this is illustrated in Fig. 3.3.

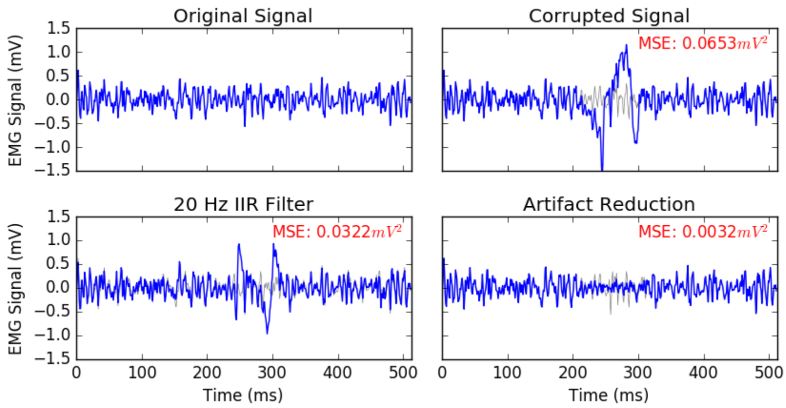

Figure 3.3: Examples of clean sEMG signal (top-left) and an artificially added motion artifact (top-right) filtered with a conventional Butterworth filter (bottom-left) and artifact reduction (bottom-right). The original signal is underlayed on each window in gray. Artifact reduction decreases the effect of the corruption (presented as MSE) much more than conventional filtering, and the signal distortion it imposes only occurs during the artifact, where the filter distorts the entire signal.

3.1.7 MLP Classifier

A Multi-Layer Perceptron classifier was written in C and optimized for the Tiva microcontroller using the CMSIS software library [53]. The predicted class value, $\hat{c}$, is estimated using equations (3.11-3.17) from an input row vector, $\overrightarrow{v}^I$

$$\overrightarrow{v}_1^H = \sigma(\boldsymbol{W}^I \overrightarrow{v}^I) \tag{3.11}$$
$$\overrightarrow{v}_2^H = \sigma(\boldsymbol{W}_1^H \overrightarrow{v}_1^H) \tag{3.12}$$
$$\overrightarrow{v}_3^H = \sigma(\boldsymbol{W}_2^H \overrightarrow{v}_2^H) \tag{3.13}$$
$$\ldots \tag{3.14}$$
$$\overrightarrow{v}_N^H = \sigma(\boldsymbol{W}_{N-1}^H \overrightarrow{v}_{N-1}^H) \tag{3.15}$$
$$\overrightarrow{v}^O = \sigma(\boldsymbol{W}^O \overrightarrow{v}_N^H) \tag{3.16}$$
$$\hat{c} = \max_C(\overrightarrow{v}^O) \tag{3.17}$$

where $\sigma(\cdot)$ denotes the element-wise activation function and $\boldsymbol{W}$ denotes the neuron weight matrix for the input (I), hidden (H), and output (O) layers.

3.2 Parameter Selection

Some preliminary analysis was performed on the effectiveness of each of the proposed denoising methods on the accuracy of the available classifications algorithms.

This analysis was used to determine which combination of the wavelet-based processing methods and machine learning algorithms showed the greatest improvement. While this limits the overall scope of this work, the number of possible parameter combinations was deemed too high to reasonably expect subjects to perform during the experiment.

3.2.1 EMG Data Acquisition

Data for the offline evaluation and selection of appropriate wavelet parameters was performed on a publicly accessible data set of 20 subjects performing 10 wrist, hand, and forearm movements recorded using 4 sets of untargeted bipolar electrodes sampled at 2 kHz [61]. Data was decimated to 1 kHz, and the 4 movements not used in the real-time analysis (side grip, fine grip, thumbs up, and pointer) were discarded to better match the real-time evaluation of the proposed algorithms, leaving the hand open and close, wrist flexion and extension, and arm pronation and supination movements for analysis. White Gaussian noise with 0 dBW power was added to each movement in the testing data and was scaled to 20% of one standard deviation of the signal for the respective movement. Training was performed using 10-fold cross validation on the data set; metrics were calculated on each parameter set 10 times using 90% of the data for training and 10% of the data for classifier testing.

3.2.2 Selection Metrics

Five metrics were used to compare the performance of each of the wavelet-based signal processing algorithms: global accuracy, processing time, the Mean Squared Error (MSE) between the original data and the filtered original data (MSE_{rec}), the MSE between the noisy filtered data and the original data (MSE_{ref}), and the MSE between the noisy filtered data and the filtered original data (MSE_{noise}). The MSE metrics were used to measure the distortion from the original signal caused by the proposed processing methods. For this experiment, lower values are better with zero being the ideal case.

3.2.3 Preliminary Analysis

As this is a window-based processing routine, the delay it introduces depends on the number of active channels and the length of the time window. Due to the nature of the wavelet transform, the operations work most efficiently on time windows with samples lengths that are a power of 2 [34]. For this experiment, a time window length of 128 ms with 64 ms overlap was selected, which falls in the typical windowing range for sEMG applications and still allows for some processing time before the control algorithm begins to feel unresponsive [9, 15]. Time performance metrics were collected for each of the proposed denoising algorithms on this window length and are shown in Fig. 3.4.
Motion artifact reduction without the use of wavelet denoising was the only set of parameters that indicated any statistically significant ($p < 0.05$) global accuracy improvement over the control, Fig. 3.5. It also showed the smallest overall signal

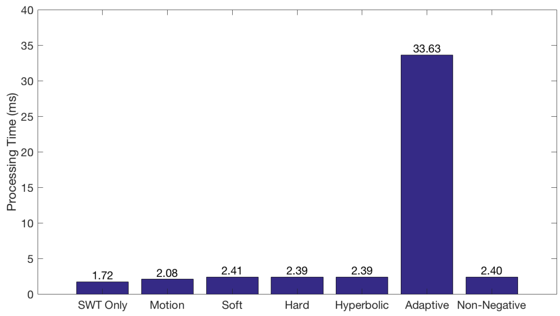

Figure 3.4: Mean processing time required for proposed denoising algorithms on 1 channel with 128 sample length windows. The label 'SWT Only' only includes the SWT and its inverse transform, 'Motion' includes the transforms and motion artifact reduction, and all others include the transforms, artifact reduction, and the listed routine.

distortion, Fig. 3.6. Adaptive thresholding showed possible improvement when used with the LDA classifier, but the processing time to perform the algorithm was prohibitively high, Fig. 3.4.

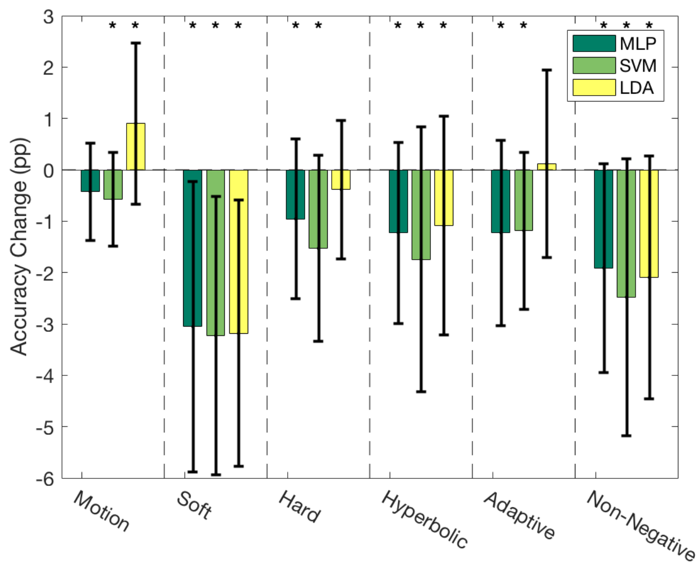

Figure 3.5: Mean offline accuracy change ± 1 SD compared with conventional filtering. Motion artifact reduction using an LDA classifier without wavelet denoising shows the only statistically significant ($p < .05$) improvement.

3.3 Experimental Evaluation

In this work, the wavelet-based signal processing and mean data imputing routines were tested separately. A test set consisted of the patient performing a motion test with the routine in question active, and another with the routine disabled.

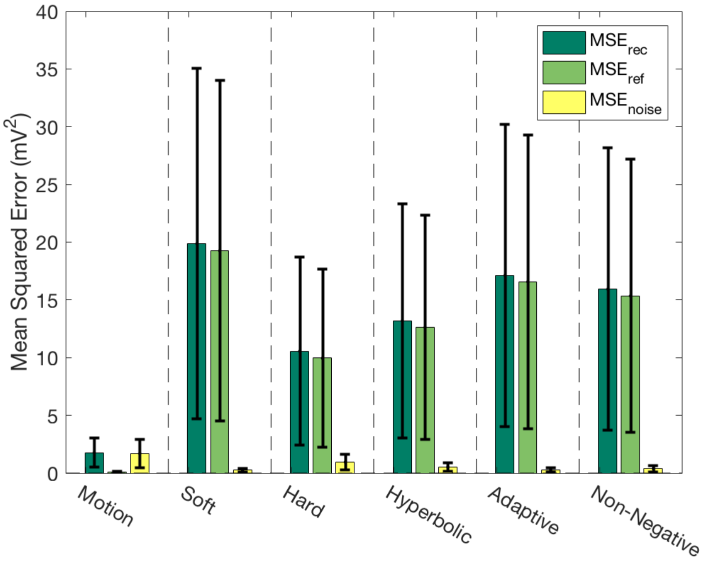

Figure 3.6: Mean offline MSE $\pm$ 1 SD compared with conventional filtering. Motion artifact reduction caused the smallest amount of overall signal distortion ($p < .05$)

All data collection, visual cueing, and pattern recognition training was controlled by the *BioPatRec* software suite running in MATLAB 2016b [62]. EMG data acquisition, signal processing, feature extraction, and movement prediction were all implemented on the artificial limb controller hardware described in [63].

3.3.1 Training Protocol

The basic training procedure for each test set consisted of patients performing contractions for each movement three times in sequence. Subjects were asked to perform each contraction at 70-80% of maximum strength for three seconds with a three second rest between each contraction. A live display of the EMG recordings was shown to the subjects during training as a form of biofeedback.

3.3.2 Motion Tests

The Motion Test, originally proposed by Kuiken *et al.* [64], was used to evaluate the effect of the proposed algorithms on the predictive capability of an LDA classifier. Each trial of a motion test consisted of a total of three random permutations of the entire movement set. Subjects were asked to perform the indicated movements with 70-80% maximum strength until either 20 correct predictions were made by the system or 10 seconds had elapsed. To offer biofeedback during the tests, subjects were shown the currently predicted value by the system in real-time.

3.3.3 Performance Metrics

Classifier accuracy, specificity, and sensitivity from the motion tests were used as performance metrics for the rest of the analysis in this work in addition to selection time, completion time, and completion rate, defined in [64]. Specificity and sensitivity were included to compensate for the inherent bias of global accuracy and to account for the large impact misclassifications can have on task completion when using prosthetic devices [41]. Data imputing tests employed an additional metric referred to in this work as the rest rate, defined as the percentage of false negative misclassifications resulting in no movement. This was used to show the difference in unintended movements resulting from LOEs produced by the proposed algorithm. All comparison between the proposed systems and the null hypotheses were performed using two-way ANOVA tests without replication.

3.4 Real-Time Tests

For the real-time tests, the order of the routines tested and the order of the test sets were both chosen at random to minimize any learning or fatigue affects on the system performance. A few minutes of rest was allowed between each set of tests to ensure the muscles were not fatigued. The electrodes were disconnected at this time, so the training protocol was performed again after the break before starting the next test set.

3.4.1 Participants

The participants for the real-time analysis of the proposed system were all healthy, able-bodied subjects between 22 and 29 years old. The mean age was 25 with a standard deviation of 2.5 years. Limb-deficient subjects were not preferentially chosen in this study, as evidence suggests that there is little difference in pattern recognition-based upper limb prosthetic controllability between limb-deficient and able-bodies subjects [65].

3.4.2 EMG Data Acquisition

Data for real-time EMG tests were collected from four sets of Ag/AgCl bipolar electrodes placed with approximately equal spacing around the proximal third of each subjects' dominant forearm. EMG signals were sampled at 2 kHz at 24-bit resolution with 24 V/V gain. The recorded data was then decimated to 1 kHz and filtered using a second order 20 Hz IIR high-pass filter and a 50 Hz IIR notch filter to minimize common-mode signals and power-line noise, respectively.

3.4.3 Wavelet-Based Signal Processing

To evaluate the performance of the proposed artifact reduction routine, the patient was instructed to perform two motion tests, one relying solely on the 20 Hz high-pass and 50 Hz notch filters, and one with the addition of wavelet-based artifact reduction.

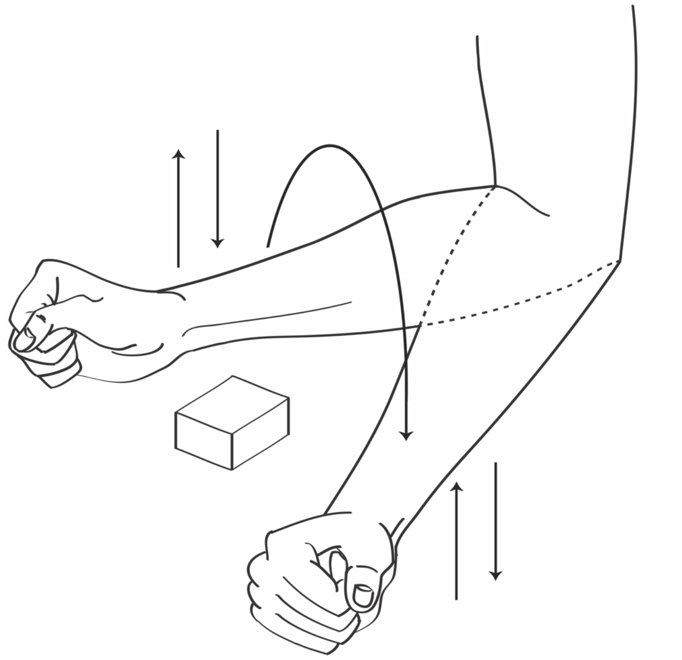

Figure 3.7: Motion artifacts were generated in real-time by having the patient bump their wrist against the table on either side of a small obstacle during each contraction [66].

Subjects were instructed to start each contraction with their elbow resting on the table and the forearm raised such that no electrodes were touching the table. They were then instructed to bump their wrist against the table once on each side of a small obstacle, pivoting on their elbow, while maintaining the contraction, illustrated in Fig. 3.7. This action is intended to simulate the typical case for sEMG signal transients where the user may bump the prosthetic against an object or shift the appendage in the socket or electrode band.

3.4.4 Data Imputing

To test the efficacy of the lead-off detection and data imputing subsystem, two motion tests were performed, one with mean data imputation enabled, and one without any extra processing. A single-pole double-throw continuity switch was fixed to each lead pair, illustrated in Fig. 3.1, and operated manually using a random number generator to indicate disconnect events. The generator indicated new events at a pseudo-random interval with a 2 second mean time between events and a standard deviation of 1 second. Disconnect events lasted for between approximately 0.2 and 0.5 seconds, and began occurring immediately after starting each test. Training data for these tests were left uncorrupted, since classifier training typically either occurs in a controlled environment or is repeatedly performed until satisfactory accuracy is reached.

3.5 Simulated Tests

To formulate robust statistics on the effectiveness of the proposed routines, an extra set of tests were performed to see how they affected the accuracy and controllability for exactly identical data sets. This was not feasible to do on live recordings, but could be done by feeding previously recorded EMG signals from motion tests into the microcontroller and recording the resulting classifications. It is referred to as a simulated test, as it is not a true real-time test, but was still implemented on the microcontroller in a similar fashion.

3.5.1 EMG Data Acquisition

The simulated tests for this experiment were performed on a subset of the data set used in [14], where EMG signals were recorded from 15 able-bodied subjects performing 10 wrist and forearm movements via 4 sets of bipolar electrodes placed with roughly equal spacing across the proximal third of the dominant forearm. This data set was recorded at 2 kHz with a second order digital high-pass filter at 20 Hz and a notch filter centered at 50 Hz. The set contained the EMG signals corresponding to both the pattern recognition training data and the full motion tests. The recorded motion tests consisted of three trials of three repetitions of each of the ten trained movements. As the EMG data for the tests were recorded using different time window parameters (resulting in a larger window incompatible with the current artifact reduction routine), only the first 128 ms in each time window, after decimating to 1 kHz, was extracted to form the training and testing sets.
The ground-truth for the simulated tests was determined by running the classifier against the recorded motion tests without simulated LOEs or motion artifacts and saving the positions of the correct classifications. Any incorrect predictions made in this situation are ignored, as the proposed algorithms are not assumed to significantly increase the predictive power of the classifiers on clean data sets.

3.5.2 Artifact Reduction

Data for comparing the artifact reduction routing with conventional filtering were modified with a set of pre-recorded motion artifacts available in the BioPatRec software suite [62]. The available motion artifacts, examples of which are shown in Fig. 3.8, were decimated and filtered to match the properties of the EMG signal. For each time window in the motion test, random artifacts were added on random channels at random offsets with magnitudes corresponding to between 1 and 10 times the standard deviation of the signal strength of that window.
Artifact reduction, when applicable, and pattern classification were performed onboard the microcontroller using a pre-trained LDA classifier by providing each time window over a serial connection and reading the resulting classifications. Artifacts were not added to the training data, but to compensate for the non-linear effects the motion artifact reduction routine has on the signal, seen in the offline analysis, the routine was applied to both the training and testing data for that case, illustrated in Fig. 3.9.

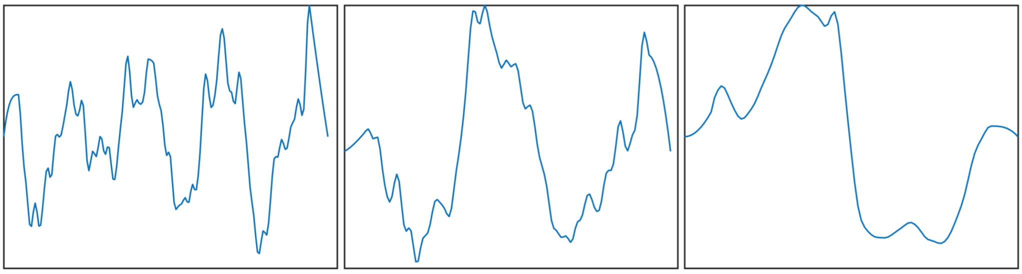

Figure 3.8: Some examples of transient artifact signals that can occur in recordings. From left to right: high-impedance, contact motion during contraction, and contact motion during rest.

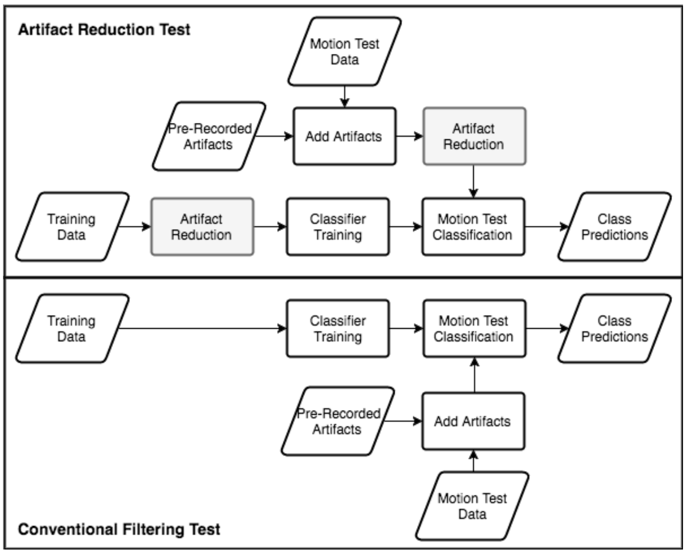

Figure 3.9: Block diagram showing the training and testing procedure used to evaluate wavelet-based motion artifact reduction on pre-recorded motion tests.

3.5.3 Data Imputing

Data for simulating lead-off events were taken from a recording of noise picked up by a set of disconnected leads recorded with the same hardware and settings as the motion test recordings listed above. The noise was then downsampled to 1 kHz and separated into 128 ms time windows. Motion test data at random time indexes on random channels on all time windows were replaced with either a random sample of recorded noise (for conventional handling) or zeros (for mean data imputing).

4
Conclusion

The offline results for the wavelet-based signal denoising schemes were not out of line with previous research. While some literature indicated a relatively small MSE between raw and processed sEMG data using the selected parameters on the MABS feature [17], little investigation has been done on features that contain more frequency information (i.e. ZC and SSC). The only other literature known to the author that showed a statistically significant increase in classification accuracy used an MLP classifier implemented with more neurons than what was considered feasible for the real-time, microcontroller-based implementation used in this experiment [18]. The use of wavelet-based denoising has yet to be investigated using nonlinear kernel functions for an SVM classifier or different neural network systems and represents an avenue for future investigation.

The intention of the real-time wavelet-based processing experiment was to show any obvious differences between the two processing methods, and none were shown. A single motion artifact typically lasts up to 100 ms [18], and given the window size, the test would show up to 6 windows corrupted by motion artifacts from hitting the table, plus any that occurred during the transit of the forearm above the table. Given that each test lasts up to 10 seconds (approximately 150 time windows), this test may not be expected to show statistical significance. The varying amount of time the processor spent on processing each time window also led to inconsistency in the results. Similar logic applies to the small difference shown when comparing conventional lead-off processing and mean data imputing.

The simulated processing tests were intended to show, at the expense of some real-world applicability, the effectiveness of the proposed algorithms in a highly reproducible setting. These results indicated statistically improved performance ($p < .001$) on most metrics with the artifact reduction routines at both the proposed wavelet levels, but greater improvement using the 3rd-level transform. Neglecting the 4th-level reduces processing time (by requiring fewer filtering operations), so use of the 3rd level routine showed the greatest potential. Simulated test results also showed a statistically significant ($p < .001$) improvement on accuracy and specificity using mean data imputing during lead-off events, but at the cost of completion rate. These results are offset by the significant increase in the rest rate, indicating that while the system completes fewer movements, the number of misclassifications resulting in unintended movements is effectively reduced. It is noteworthy to emphasize that at least one channel was corrupted with a lead-off event on every time window, so these results serve as a worst-case scenario, rather than a typical use-case. These results suggest that mean data imputing is an effective strategy for handling LOEs during continuous sEMG classification.

The prospects of myoelectric control systems continually improves as the discrepancy between signal processing and analysis and robotic systems decreases. Investigation into the efficient, low-cost implementation of these control systems is crucial to the development of EMG-based assistive devices, as without the mobility offered by small, low-power control systems, the applicability of advanced processing methods and control strategies is severely limited. As such, while the MLP classifier did not prove useful in evaluating the performance of wavelet-based denoising, having an efficient implementation of it working on the microcontroller enables the use of it in future analysis. Wavelet denoising has already been demonstrated to be useful in spike-sorting schemes, so the system may prove to be useful for TMR recipients [23].

Wavelet-based artifact reduction and mean data imputation have been shown in this work to be effective at increasing the robustness of pattern recognition-based, upper-limb EMG control systems. No attempt has been made, yet, to investigate whether the proposed system would increase overall controllability and end-user trust in daily activities. Integrating these algorithms on a portable system compatible with existing robotic hands has been a critical step in allowing the appropriate tests to be conducted.

Bibliography

[1] Ahmet Alkan and Mücahid Günay. Identification of EMG signals using discriminant analysis and SVM classifier. *Expert Systems with Applications*, 39(1):44–47, 2012.

[2] Theodore a Kung, Reuben a Bueno, Ghadah K Alkhalefah, Nicholas B Langhals, Melanie G Urbanchek, and Paul S Cederna. Innovations in prosthetic interfaces for the upper extremity. *Plastic and reconstructive surgery*, 132(6):1515–1523, 2013.

[3] Elaine Biddiss, Dorcas Beaton, and Tom Chau. Consumer design priorities for upper limb prosthetics. *Disability and Rehabilitation: Assistive Technology*, 2(6):346–357, 2007.

[4] Adriano O. Andrade, Adriano A. Pereira, Steffen Walter, Rosimary Almeida, Rui Loureiro, Diego Compagna, and Peter J. Kyberd. Bridging the gap between robotic technology and health care. *Biomedical Signal Processing and Control*, 10(1):65–78, 2014.

[5] Aidan Roche, Hubertus Rehbaum, Dario Farina, and Oskar Aszmann. Prosthetic Myoelectric Control Strategies: A Clinical Perspective. *Current Surgery Reports*, 2(3):1–11, 2014.

[6] Anders Fougner, Øyvind Stavdahl, Peter J Kyberd, Yves G Losier, Philip A Parker, and Senior Member. Control of Upper Limb Prostheses : Terminology and Proportional Myoelectric Control — A Review. *IEEE TRANSACTIONS ON NEURAL SYSTEMS AND REHABILITATION ENGINEERING*, 20(5):663–677, 2012.

[7] Dario Farina, Ning Jiang, Hubertus Rehbaum, Aleš Holobar, Bernhard Graimann, Hans Dietl, and Oskar C. Aszmann. The extraction of neural information from the surface EMG for the control of upper-limb prostheses: Emerging avenues and challenges. *IEEE Transactions on Neural Systems and Rehabilitation Engineering*, 22(4):797–809, 2014.

[8] Silvestro Micera, Jacopo Carpaneto, and Stanisa Raspopovic. Control of Hand Prostheses Using Peripheral Information. *IEEE REVIEWS IN BIOMEDICAL ENGINEERING*, 3:48–68, 2010.

[9] Mohammadreza Asghari Oskoei and Huosheng Hu. Myoelectric control systems-A survey. *Biomedical Signal Processing and Control*, 2(4):275–294, 2007.

[10] Ivan Vujaklija, Dario Farina, and O Aszmann. New developments in prosthetic arm systems. *Orthop. Res. Rev*, 8:31–39, 2016.

[11] Dario Farina and Oskar Aszmann. Bionic limbs: clinical reality and academic promises. *Science translational medicine*, 6(257):257ps12–257ps12, 2014.

[12] Xiaorong Zhang and He Huang. A real-time, practical sensor fault-tolerant module for robust EMG pattern recognition. *Journal of NeuroEngineering and Rehabilitation*, 12(1):18, 2015.

[13] Bart Peerdeman, Daphne Boere, Heidi Witteveen, Rianne Huis in 't Veld, Hermie Hermens, Stefano Stramigioli, Hans Rietman, Peter Veltink, and Sarthak Misra. Myoelectric forearm prostheses: state of the art from a user-centered perspective. *Journal of rehabilitation research and development*, 48(6):719–37, 2011.

[14] Max Jair Ortiz-Catalan. *Towards Natural Control of Artificial Limbs*. PhD thesis, Chalmers University of Technology, 2014.

[15] Maria Hakonen, Harri Piitulainen, and Arto Visala. Current state of digital signal processing in myoelectric interfaces and related applications. *Biomedical Signal Processing and Control*, 18:334–359, 2015.

[16] E. A. Clancy, E. L. Morin, and R. Merletti. Sampling, noise-reduction and amplitude estimation issues in surface electromyography. *Journal of Electromyography and Kinesiology*, 12(1):1–16, 2002.

[17] Angkoon Phinyomark, Chusak Limsakul, and Pornchai Phukpattaranont. A comparative study of wavelet denoising for multifunction myoelectric control. In *Computer and Automation Engineering, 2009. ICCAE'09. International Conference on*, pages 21–25. IEEE, 2009.

[18] Julian Maier. *Wavelet Transform-based Algorithms for Myoelectric Control*. PhD thesis, University of Stuttgart, 2016.

[19] MBI Reaz, MS Hussain, Faisal Mohd-Yasin, et al. Techniques of emg signal analysis: detection, processing, classification and applications. *Biological procedures online*, 8(1):11–35, 2006.

[20] Mark Ison and Panagiotis Artemiadis. The Role of Muscle Synergies in Myoelectric Control: Trends and Challenges for Simultaneous Multifunction Control. *Journal of Neural Engineering*, 11(5):051001, 2014.

[21] Angkoon Phinyomark, Chusak Limsakul, and Pornchai Phukpattaranont. Application of wavelet analysis in emg feature extraction for pattern classification. *Measurement Science Review*, 11(2):45–52, 2011.

[22] Kevin Englehart, B Hudgin, and Philip A Parker. A wavelet-based continuous classification scheme for multifunction myoelectric control. *IEEE Transactions on Biomedical Engineering*, 48(3):302–311, 2001.

[23] Danilo Pani, Gianluca Barabino, Student Member, Luca Citi, Paolo Meloni, Stanisa Raspopovic, Silvestro Micera, Senior Member, and Luigi Raffo. Real-Time Neural Signals Decoding onto Off-the-Shelf DSP Processors for Neuroprosthetic Applications. 24(9):993–1002, 2016.

[24] Angkoon Phinyomark, Pornchai Phukpattaranont, and Chusak Limsakul. Feature reduction and selection for EMG signal classification. *Expert Systems with Applications*, 39(8):7420–7431, 2012.

[25] OpenStax. Motor end plate and innervation. `https://upload.wikimedia.org/wikipedia/commons/5/57/1009_Motor_End_Plate_and_Innervation.jpg`, 2016. This work is a derivative of the original created under CC BY 4.0.

[26] Dario Farina and Ales Holobar. Human machine interfacing by decoding the surface electromyogram. *IEEE Signal Processing Magazine*, 32(1):115–120, 2015.

[27] Guanglin Li, Yaonan Li, Long Yu, and Yanjuan Geng. Conditioning and sampling issues of emg signals in motion recognition of multifunctional myoelectric prostheses. *Annals of biomedical engineering*, 39(6):1779–1787, 2011.

[28] Rodrigo Lício Ortolan, Ricardo Naoki Mori, Roberto R Pereira, Cristina MN Cabral, José Carlos Pereira, and Alberto Cliquet. Evaluation of adaptive/non-adaptive filtering and wavelet transform techniques for noise reduction in emg mobile acquisition equipment. *IEEE transactions on neural systems and rehabilitation engineering*, 11(1):60–69, 2003.

[29] Ping Zhou, Madeleine M Lowery, RF Weir, and Todd A Kuiken. Elimination of ecg artifacts from myoelectric prosthesis control signals developed by targeted muscle reinnervation. In *Engineering in Medicine and Biology Society, 2005. IEEE-EMBS 2005. 27th Annual International Conference of the*, pages 5276–5279. IEEE, 2006.

[30] Padma Akkiraju and DC Reddy. Adaptive cancellation technique in processing myoelectric activity of respiratory muscles. *IEEE Transactions on Biomedical Engineering*, 39(6):652–655, 1992.

[31] Guohua Lu, John-Stuart Brittain, Peter Holland, John Yianni, Alexander L Green, John F Stein, Tipu Z Aziz, and Shouyan Wang. Removing ecg noise from surface emg signals using adaptive filtering. *Neuroscience letters*, 462(1):14–19, 2009.

[32] C Marque, C Bisch, R Dantas, S Elayoubi, V Brosse, and C Perot. Adaptive filtering for ecg rejection from surface emg recordings. *Journal of electromyography and kinesiology*, 15(3):310–315, 2005.

[33] Michelle Rene Davies and SS Reisman. Time frequency analysis of the electromyogram during fatigue. In *Bioengineering Conference, 1994., Proceedings of the 1994 20th Annual Northeast*, pages 93–95. IEEE, 1994.

[34] Guy P Nason and Bernard W Silverman. The stationary wavelet transform and some statistical applications. In *Wavelets and statistics*, pages 281–299. Springer, 1995.

[35] AN Akansu, WA Serdijn, and IW Selesnick. Wavelet transforms in signal processing: a review of emerging applications. *Physical Communication, Elsevier*, 3(1):1–18, 2010.

[36] S Grimnes. Impedance measurement of individual skin surface electrodes. *Medical and Biological Engineering and Computing*, 21(6):750–755, 1983.

[37] Ann M Simon, Levi J Hargrove, Blair A Lock, and Todd A Kuiken. A decision-based velocity ramp for minimizing the effect of misclassifications during real-time pattern recognition control. *IEEE Transactions on Biomedical Engineering*, 58(8):2360–2368, 2011.

[38] Pedro J García-Laencina, José-Luis Sancho-Gómez, and Aníbal R Figueiras-Vidal. Pattern classification with missing data: a review. *Neural Computing and Applications*, 19(2):263–282, 2010.

[39] Kristiaan Pelckmans, Jos De Brabanter, Johan AK Suykens, and Bart De Moor. Handling missing values in support vector machine classifiers. *Neural Networks*, 18(5):684–692, 2005.

[40] Mark Laubach. Wavelet-based processing of neuronal spike trains prior to discriminant analysis. *Journal of neuroscience methods*, 134(2):159–168, 2004.

[41] Sophie M Wurth and Levi J Hargrove. A real-time comparison between direct control, sequential pattern recognition control and simultaneous pattern recognition control using a fitts' law style assessment procedure. *Journal of neuroengineering and rehabilitation*, 11(1):91, 2014.

[42] Todd R Farrell and Richard F Weir. The optimal controller delay for myoelectric prostheses. *IEEE Transactions on neural systems and rehabilitation engineering*, 15(1):111–118, 2007.

[43] Bernard Hudgins, Philip Parker, and Robert N Scott. A new strategy for multifunction myoelectric control. *IEEE Transactions on Biomedical Engineering*, 40(1):82–94, 1993.

[44] Mohammadreza Asghari Oskoei and Huosheng Hu. Support vector machine-based classification scheme for myoelectric control applied to upper limb. *IEEE transactions on biomedical engineering*, 55(8):1956–1965, 2008.

[45] Silvestro Micera, Angelo M Sabatini, Paolo Dario, and Bruno Rossi. A hybrid approach to emg pattern analysis for classification of arm movements using statistical and fuzzy techniques. *Medical engineering & physics*, 21(5):303–311, 1999.

[46] Bernhard E Boser, Isabelle M Guyon, and Vladimir N Vapnik. A training algorithm for optimal margin classifiers. In *Proceedings of the fifth annual workshop on Computational learning theory*, pages 144–152. ACM, 1992.

[47] Sebastian Bitzer and Patrick Van Der Smagt. Learning emg control of a robotic hand: towards active prostheses. In *Robotics and Automation, 2006. ICRA 2006. Proceedings 2006 IEEE International Conference on*, pages 2819–2823. IEEE, 2006.

[48] Simon Haykin and Neural Network. A comprehensive foundation. *Neural Networks*, 2(2004):41, 2004.

[49] Matt J Kusner, Stephen Tyree, Kilian Weinberger, and Kunal Agrawal. Stochastic Neighbor Compression. *Jmlr W&Cp*, 32(1):622–630, 2014.

[50] Sharadh Ramaswamy and Kenneth Rose. Adaptive cluster distance bounding for high-dimensional indexing. *IEEE Transactions on Knowledge and Data Engineering*, 23(6):815–830, 2011.

[51] S Dhanabal and S Chandramathi. A Review of various k-Nearest Neighbor Query Processing Techniques. *International Journal of Computer Applications*, 31(7):14–22, 2011.

[52] Abidemi Bolu Ajiboye and R Fff Weir. A heuristic fuzzy logic approach to emg pattern recognition for multifunctional prosthesis control. *IEEE Transactions on Neural Systems and Rehabilitation Engineering*, 13(3):280–291, 2005.

[53] ARM Holdings plc. Cortex microcontroller software interface standard. `https://github.com/ARM-software/CMSIS_5`, 2017. This work was created under the Apache-2.0 license.

[54] David L Donoho, Iain M Johnstone, et al. Ideal denoising in an orthonormal basis chosen from a library of bases. *Comptes rendus de l'Académie des sciences. Série I, Mathématique*, 319(12):1317–1322, 1994.

[55] Qu Tianshu, Wang Shuxun, Chen Haihua, and Dai Yisong. Adaptive denoising based on wavelet thresholding method. In *Signal Processing, 2002 6th International Conference on*, volume 1, pages 120–123. IEEE, 2002.

[56] Li Su, Guoliang Zhao, and Renyan Zhang. Translation-invariant wavelet denoising method with improved thresholding. In *Communications and Information Technology, 2005. ISCIT 2005. IEEE International Symposium on*, volume 1, pages 619–622. IEEE, 2005.

[57] Brani Vidakovic. *Statistical modeling by wavelets*, volume 503. John Wiley & Sons, 2009.

[58] Hong-Ye Gao. Wavelet shrinkage denoising using the non-negative garrote. *Journal of Computational and Graphical Statistics*, 7(4):469–488, 1998.

[59] Charles M Stein. Estimation of the mean of a multivariate normal distribution. *The annals of Statistics*, pages 1135–1151, 1981.

[60] Sandeep P Ghael, Akbar M Sayeed, and Richard G Baraniuk. Improved wavelet denoising via empirical wiener filtering. In *Optical Science, Engineering and Instrumentation'97*, pages 389–399. International Society for Optics and Photonics, 1997.

[61] Max Jair Ortiz-Catalan. Biopatrec data repository, 2016. `https://github.com/biopatrec/biopatrec/tree/Data_Repository/10mov4chForearmUntargeted/`.

[62] Max Jair Ortiz-Catalan. Biopatrec, 2016. `https://github.com/biopatrec/biopatrec`.

[63] E. Mastinu, P. Doguet, Y. Botquin, B. Håkansson, and M. Ortiz-Catalan. Embedded system for prosthetic control using implanted neuromuscular interfaces accessed via an osseointegrated implant. *IEEE Transactions on Biomedical Circuits and Systems*, PP(99):1–11, 2017.

[64] Todd A Kuiken, Blair A Lock, Robert D Lipschutz, Laura A Miller, Kathy A Stubblefield, and Kevin B Englehart. Targeted Muscle Reinnervation for Real-time Myoelectric Control of Multifunction Artificial Arms. *Journal of the American Medical Association*, 301(6):619–628, 2009.

[65] Erik Scheme and Kevin Englehart. Electromyogram pattern recognition for control of powered upper-limb prostheses: State of the art and challenges for clinical use. *Journal of Rehabilitation Research and Development*, 48(6):643–660, 2011.

[66] Jennifer Bowman. Motion artifact generation illustration, 2017. This work was created under CC BY NC-SA.

A
Scientific Paper

Stationary Wavelet Processing and Data Imputing in Myoelectric Pattern Recognition on a Low-Cost Embedded System

Adam Naber, Enzo Mastinu, *Student Member, IEEE*, Max Ortiz-Catalan, *Member, IEEE*

***Abstract*—Surface electromyography offers a low-cost, non-invasive method of decoding motor intention for prosthetic control. Pattern recognition-based approaches to decoding muscle signals allow for advanced, intuitive control, but at the cost of sensitivity to in-band noise and sensor faults. The controllability and robustness of such systems can be improved with wavelet-based signal processing and data imputing. Research has largely focused on offline analysis of recorded data using these processing algorithms, and no attempt has been made to investigate the feasibility of executing them on a portable system in real-time. The aim of this work was to investigate the feasibility of low-latency wavelet-based signal processing and data imputing on an embedded device capable of controlling upper-arm prostheses. Nine able-bodied subjects were asked to perform Motion Tests in the presence of transient in-band noise and sensor faults. Minor differences were found between conventional and advanced processing due to the low number of disturbance episodes. In order to observe the effect of a higher number of episodes, further investigation was performed on a set of pre-recorded Motion Tests from 15 able-bodied subjects with artificially added noise and sensor faults. The tests with simulated interferences showed a statistically significant increase in classifier accuracy, specificity, sensitivity, and precision for wavelet processing as well as an increase in accuracy, specificity, and precision for data imputing. These results suggest that the proposed routines can be implemented in real-time systems to improve prosthetic device controllability and that they are viable for use in further studies in daily life activities.**

***Index Terms*—prosthetic limbs, myoelectric pattern recognition, stationary wavelet transform, data imputing, signal de-noising**

I. Introduction

ELECTROMYOGRAPHY (EMG) signals from vestigial muscles are the most common control source for powered prostheses, due to their direct correlation to motor intention and ease of non-invasive detection [1]. There is a significant discrepancy between the current mechatronic prosthetic technology and the fidelity of the signal acquisition and control systems. This results in limited controllability and frequent frustration from users [2]. A study performed in 2007 showed 39 % of upper-limb amputees with direct control myoelectric prostheses did not use them regularly due to issues stemming primarily from low controllability and functionality [3], though the relationship between lost limb functionality and user requirements is complex and changes over time [4]. Artificial limb rejection rates have not decreased, despite the addition of proportional speed control and the adoption of functional hand grips by many manufacturers [3], [5], [6]. This suggests a more intuitive control mechanism is required to address patient needs.

Using myoelectric pattern recognition (MPR) to predict motor intention from multi-channel surface EMG (sEMG) is a more intuitive alternative to direct control. MPR removes the need for switching between different degrees of freedom and allows for more natural motion. The increased functionality MPR systems provide is offset by a large reduction in robustness. This is an important consideration, as an incorrect movement of the prosthetic at any point can compromise an entire task [7]. The clinical translation of such technology has been hindered by the lack of robustness. Environmental noise, signal artifacts caused by electrode movement, and missing and corrupted signals due to loose electrode-skin contact have the greatest negative impact on MPR systems using sEMG [8], [9]. Methods that reduce their impact can have a significant positive affect on the controllability, robustness, and eventual adoption of clinical prostheses.

The aforementioned noise sources have wide-band and non-stationary characteristics, making them difficult to remove with FIR or IIR filters without also removing useful signal components. Using more electrodes can offset some of their effects in cases of transient noise or lead-off events, where the issue may only affect one channel, but this also increases the system complexity and is only useful if there are enough available myoelectric sites. The burden of detecting and compensating for these noise sources then falls to more advanced signal processing.

Wavelet-based signal analysis has been gaining significant popularity in treating complex, noisy biological signals. Several works have been published on using subsets of wavelet transform coefficients directly in sEMG pattern recognition systems that demonstrate an increase in classification accuracy [9], [10]. Other works have focused on using the wavelet transform to dynamically reduce noise across the time and frequency domains based on *a priori* knowledge about the signal and noise sources, referred to as de-noising [11]–[15]. The latter approach produces a cleaned version of the original signal, providing a more direct correlation between

Research was supported by the Promobilia foundation, VINNOVA, and Swedish Research Council (Vetenskapsrådet)

Adam Naber is with the Dept. of Electrical Engineering, Chalmers University of Technology, Gothenburg, Sweden (e-mail: naber@student.chalmers.se)

E. Mastinu is with the Dept. of Elecrical Engineering, Chalmers University of Technology, Gothenburg, Sweden (e-mail: enzo@chalmers.se)

M. Ortiz-Catalan is with the Dept. of Electrical Engineering, Chalmers University of Technology, and Integrum AB, Gothenburg, Sweden (e-mail: maxo@chalmers.se)

the result and motor intention, and allowing for straightforward integration in existing systems. To the authors' knowledge, no investigation has been made into determining the feasibility of implementing a real-time signal de-noising routine on an microcontroller operating independently of a PC. Demonstrating the feasibility of executing such algorithms in real-time and in an embedded system is the next logical step towards more robust pattern recognition-based control in limb prostheses.

The aforementioned algorithms do not address the situation where electrodes lose their electrical coupling with the body, which is another potential complication on myoelectric prostheses. Little is known on the occurrence of such situations in daily use, but their effects are significant enough for lead-off event (LOE) detection circuitry to be included in many bio-potential amplifiers. The result of an LOE is a complete loss of EMG often coupled with strong transients as electrodes disconnect and reconnect with the skin.

Existing classifiers that adapt to slow changes in signal characteristics have limited usefulness in handling LOEs, but it may not be necessary to stop classification depending on the amount of redundancy contained in the remaining sensor data [16]. Zhang *et al.* demonstrated that a Linear Discriminant Analysis-based classifier tolerant to electrode faults results in increased classification accuracy. This suggests that the signal corruption and loss of information during LOEs is a cause for concern [17]. Their implementation used a fast retraining algorithm for the classifier that compensated for missing channels. While promising, it does not provide a generic solution applicable across different machine learning algorithms.

Pelckmans *et al.* [18] suggested using a probabilistic model of missing data for support vector machines that approaches mean data imputing in the case of a linear system [16]. While the research has not been applied to sEMG signals specifically, it offers a generic solution that is computationally efficient. Since this operates directly on the signal during preprocessing, it can be implemented in a modular fashion on an existing embedded system without significant modifications.

In the present study, we investigated signal de-noising and data imputing algorithms to enhance the robustness of pattern recognition against noise and sensor faults during continuous sEMG classification. We evaluated classification accuracy on three common classifiers and signal distortion with respect to de-noising algorithms, demonstrated the feasibility of executing these algorithms in real-time and in an embedded system, and demonstrated an increase in classifier controllability from wavelet-based processing and data imputing. Our system was implemented on a low power microcontroller, allowing for further clinical translation.

II. Methods

A. Wavelet-Based Signal De-Noising

The characteristics of sEMG signals depend many factors, but the dominant frequency band viable for wavelet analysis is in the 125-250 Hz range [9], with components in the 250-500 Hz range dominated by system noise [19]. For this application, the system noise was treated as a locally-stationary additive function based on the standard deviation of the first-level (250-500 Hz) wavelet detail coefficients. Algorithms to reduce system noise from wavelet coefficients were selected based on reviews in previous literature with an emphasis on computational simplicity [12], [20]–[24]. Hard, soft, semi-hyperbolic, adaptive, and non-negative shrinkage methods were investigated in this experiment, defined in Tab. I. The Daubechies four tap wavelet was chosen as the mother wavelet due to its ability to effectively describe both time and frequency signal components and its low filter order [13]. The noise threshold parameter, λ, for each routine was calculated using the minimax threshold defined in (1):

TABLE I
Wavelet shrinkage rules evaluated in this experiment.

Rule	Formula
Hard	$\hat{\gamma}_{j,i} = \begin{cases} \gamma_{j,i}, & \lvert\gamma_{j,i}\rvert > \lambda \\ 0, & \text{otherwise} \end{cases}$
Soft	$\hat{\gamma}_{j,i} = \begin{cases} \gamma_{j,i} - \lambda, & \lvert\gamma_{j,i}\rvert > \lambda \\ 0, & \text{otherwise} \end{cases}$
Hyperbolic	$\hat{\gamma}_{j,i} = \begin{cases} \text{sgn}(\gamma_{j,i})\sqrt{\gamma_{j,i}^2 - \lambda}, & \lvert\gamma_{j,i}\rvert > \lambda \\ 0, & \text{otherwise} \end{cases}$
Adaptive	$\hat{\gamma}_{j,i} = \gamma_{j,i} - \lambda + \frac{2\lambda}{1+\exp(2.1\gamma_{j,i}/\lambda)}$
Non-Negative	$\hat{\gamma}_{j,i} = \begin{cases} \gamma_{j,i} - \frac{\lambda^2}{\gamma_{j,i}}, & \lvert\gamma_{j,i}\rvert > \lambda \\ 0, & \text{otherwise} \end{cases}$

$\gamma_{j,i} :=$ original wavelet coefficient at level j at time index i
$\hat{\gamma}_{j,i} :=$ de-noised wavelet coefficient at level j at time index i

$$\lambda = \hat{\sigma} \cdot \left(0.3936 + 0.1829 \cdot \frac{\log(N)}{\log(2)}\right) \tag{1}$$

where $\hat{\sigma}$ is the standard deviation of the system signal noise wavelet coefficients and N is the window length in samples. This is designed to minimize the maximum mean squared error against an ideal procedure [25].

B. Wiener Correction Factor

The wavelet transform concentrates the signal energy into a relatively small number of high-valued coefficients [26]. Wavelet-based de-noising then reduces the sufficiently small coefficients (assumed to be noise) towards zero, reducing the signal subspace (the number of non-zero coefficients used to describe the signal). This property, combined with the fact that the wavelet transform provides rich spectral characteristics on both the desired signal and the noise lends the process to Wiener filtering, expressed as $\tilde{\gamma}_{j,i}$ in:

$$\tilde{\gamma}_{j,i} = \frac{\gamma_{j,i} \cdot \hat{\gamma}_{j,i}^2}{\hat{\gamma}_{j,i}^2 + s(\hat{\gamma}_1)^2}, \tag{2}$$

where $s(\cdot)$ denotes the corrected sample standard deviation. This treats the desired signal and the noise as locally stationary systems, which is appropriate for sufficiently small windows on isometric contractions [27], and provides a smoother system response than wavelet shrinkage alone. The Wiener filtering coefficients can be calculated on a different transform level and mother wavelet selection than the original data, Fig. 1, but this flexibility was foregone in the implementation to minimize processing time.

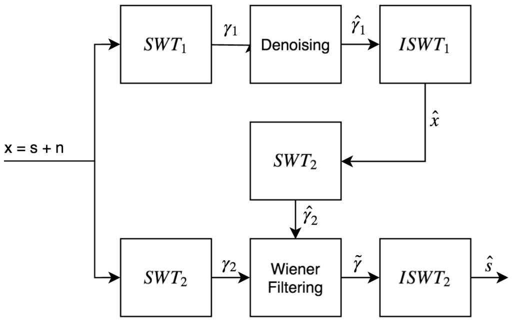

Fig. 1. Block diagram for generic wavelet-based Wiener filtering. The transforms for the Wiener coefficient estimation and for the signal filtering are separate, allowing for use of different wavelet parameters in wavelet shrinkage and Wiener filtering.

C. Wavelet-Based Artifact Reduction

Motion artifacts are characterized by strong, transient signal interference at low frequencies [8]. A third- or fourth-order wavelet transform should cleanly separate the artifacts into the approximation coefficients, corresponding to the 0-62.5 Hz and 0-31.25 Hz ranges, respectively. In this implementation, it was assumed that any sufficiently strong signal in the approximation coefficients of the transform was caused by a transient artifact. Hard thresholding was applied to each signal band (4-5) to remove the corrupted portions of the signal to produce the cleaned approximation and detail coefficients $\hat{\gamma}_{A,i}$ and $\hat{\gamma}_{D,i}$, respectively:

$$\theta_k = \mu_i(|\gamma_{\text{dom}}|) + k * s_i(\gamma_{\text{dom}}) \tag{3}$$

$$\hat{\gamma}_{A,i} = \begin{cases} \gamma_{A,i}, & \text{if } |\gamma_{A,i}| < \theta_1 \\ 0, & \text{otherwise} \end{cases} \tag{4}$$

$$\hat{\gamma}_{D,i} = \begin{cases} \gamma_{D,i}, & \text{if } |\gamma_{A,i}| < \theta_1 \cup |\gamma_{D,i}| < \theta_0 \\ 0, & \text{otherwise} \end{cases} \tag{5}$$

where $\gamma_{A,i}$ is the i-th wavelet approximation coefficient, $\gamma_{D,i}$ is the corresponding detail coefficient at decomposition level D, $\mu_i(\cdot)$ is the mean value operator, and γ_{dom} is the wavelet decomposition level corresponding to the dominant sEMG signal frequency band. The effect of this proposed algorithm is illustrated in Fig. 2.

D. Wavelet Processing Implementation

At the time of the experiment, the authors were unaware of any microcontroller compatible implementation of the SWT algorithm and its inverse. The appropriate routines were written in C, leveraging the Cortex Microcontroller Software Interface Standard for optimization of filtering operations [28]. The de-noising and artifact reduction routines were performed immediately prior to feature extraction on each sample window. Signals were reconstructed by recursively averaging all possible shifted, decimated inverse discrete wavelet transforms on each wavelet level, referred to as the average basis inverse [29].

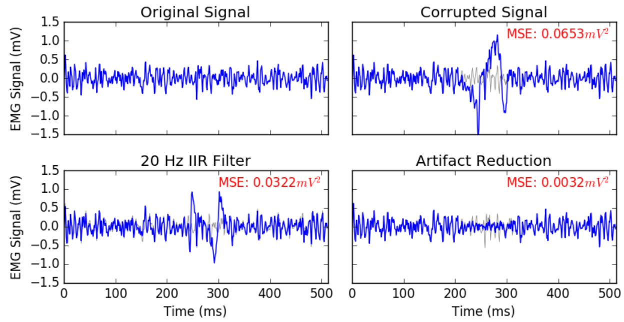

Fig. 2. Examples of clean sEMG signal (top-left) and a superimposed motion artifact (top-left) filtered with a conventional Butterworth filter (bottom-left) and artifact reduction (bottom-right). The original signal is underlayed on each window in gray. Artifact reduction decreases the effect of the corruption (presented as MSE) much more than conventional filtering, and signal distortion it imposes only occurs during the artifact, where the filter distorts the entire signal.

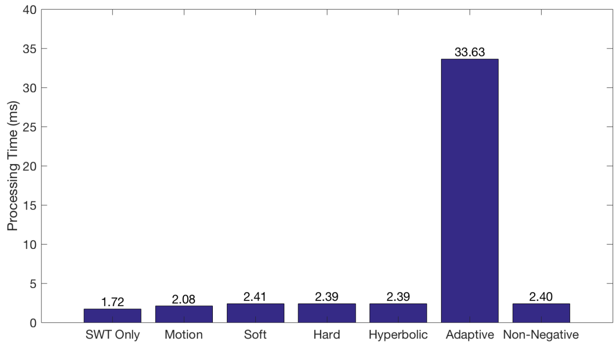

Fig. 3. Mean processing time required for each algorithm on one channel with 128 sample length windows. The label 'SWT Only' only includes the SWT and its inverse transform, 'Motion' includes the transforms and motion artifact reduction, and all others include the transforms, artifact reduction, and the listed routine.

Due to the nature of the wavelet transform, the operations work most efficiently on time windows with samples lengths that are a power of 2. For this work, a time window of 128 ms with 64 ms overlap was selected, which falls in the typical windowing range for sEMG applications and still allows for some processing time before the control algorithm begins to feel unresponsive [1], [30]. Time performance metrics were collected for each of the proposed de-noising algorithms on this window length and are shown in Fig. 3. The processing time was found to grow approximately linearly with the number of active channels and the length of the channels.

E. Lead-Off Detection and Data Imputing Implementation

Electrode disconnect events create high impedance mismatch between the amplifier and the leads. The analog front-end used in this study detects these events by adding a 6 nA DC current source to both the positive and negative leads of each bipolar terminal and setting the input impedance for each amplifier to 500 MΩ, illustrated in Fig. 4. During normal operation, the current is harmlessly dissipated through both the patient and the amplifier, but saturates the amplifier input when either or both leads are disconnected from the patient.

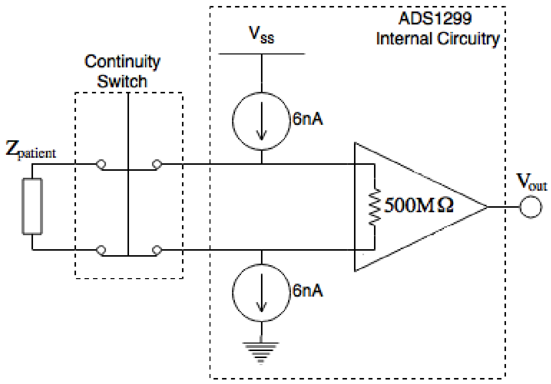

Fig. 4. Equivalent circuit for detection and simulation of lead-off events in real-time.

Hard thresholding was applied to any signal outside the 30-70 % maximum value range of the amplifier, corresponding to approximately ± 66 μV. Signals that are outside of this range were replaced with 0. This was not expected to increase the overall controllability of the system, but rather to decrease the chance of misclassifications resulting in movement when insufficient data is available for decoding motor intention.

F. Feature Extraction and Classification

The Time Domain feature set proposed by Hudgins *et al.* contains some of the most commonly investigated features in EMG applications due to their low computational complexity and high descriptivenes. [31]. A relative comparison of these and other common features suggests the use of this set (composed of mean absolute value (MABS), zero crossings (ZC), waveform length (WL), and signed slope change (SSC)) is adequate for MPR [32], [33].

The processing and memory requirements of many pattern recognition systems limits the selection for real-time embedded applications. Multi-Layer Perceptron (MLP), Support Vector Machine (SVM), and Linear Discriminant Analysis (LDA) are all commonly used for EMG classification [34] and meet the constraints for real-time implementation in an embedded system. We implemented multi-class SVM and LDA classifiers using a "one-vs-all" scheme. The MLP classifier used one layer of 16 hidden neurons using the *hyperbolic tangent* activation function and the *softmax* activation function on the output neruons. The NetLab 3.3 Neural Network library was used for MLP classifier training on a PC [35]. The signal detection threshold was calculated using the average MABS feature value across all rest signal windows in the training data. Any signals with a MABS feature smaller than this value bypassed the classifier and were considered a rest state.

G. Training Protocol

The training data sets for the pattern recognition algorithms consisted of recordings of three, three second contractions for each movement with each contraction separated by three seconds of rest. Patients were asked to perform contractions at 70-80 % of their maximum voluntary contraction strength. The dynamic portions of each contraction were discarded such that only the center 75 % of the data in each contraction was preserved. Data for training the rest classification and floor noise were obtained from the center 50 % of each of the rest periods in the recordings. EMG data were separated and concatenated into arrays corresponding to the signal in each movement. The data arrays were then windowed, and signal features calculated from those windows were used to construct training, testing, and validation sets for the classifiers. Visual cueing for contractions, signal recording, and feature extraction for classifier training were all performed using BioPatRec running on MATLAB 2016b [36].

H. Experiment I. Offline Wavelet Parameter Selection

The sEMG recordings for evaluation and selection of appropriate wavelet parameters were obtained from a publicly accessible data set of 20 subjects performing 10 wrist, hand, and forearm movements [36]. The signals were recorded using four sets of untargeted bipolar electrodes sampled at 2 kHz. Data were decimated to 1 kHz and the four movements not used in the real-time analysis were discarded. Hand open and close, wrist flexion and extension, and arm pronation and supination movements were used for analysis. White Gaussian noise with 0 dBW power was added to each movement in the testing data and was scaled to 20 % of one standard deviation of the signal magnitude for the respective movement. Classifier training data was composed of a random selection 90 % of the feature windows in each movement, and testing and validation data was pooled together in the remaining 10 %. 10-fold data cross-validation was used to generalize the classifier accuracy results.

Four metrics were used to compare the performance of each of the wavelet-based signal processing algorithms: global accuracy, the Mean Squared Error (MSE) between the original data and the filtered original data (MSE_{rec}), the MSE between the filtered noisy data and the original data (MSE_{ref}), and the MSE between the filtered noisy data and the filtered original data (MSE_{noise}). To reduce the burden of subject testing to a reasonable level, only the best performing model in this test was considered for the remainder of the experiment.

I. Experiment II. Real-Time

Real-time EMG signals were collected from nine able-bodies subjects fitted with four sets of Ag-AgCL bipolar electrodes placed with approximately equal spacing around the proximal third of each subject's dominant forearm. EMG signals were sampled at 2 kHz, 24-bit resolution, and 24 V/V gain. The EMG signals were then decimated to 1 kHz and filtered using a second order 20 Hz IIR high-pass filter and a 50 Hz IIR notch filter [37].

To evaluate the performance of the proposed wavelet processing routine, the patients were instructed to perform two Motion Tests, described in section II-K, one relying solely on the 20 Hz high-pass and 50 Hz notch filters, and one with the addition of wavelet processing operating on the fourth-level transform. Subjects were instructed to start each contraction with their elbow resting on the table and the forearm raised such that no leads were touching the table. They were then

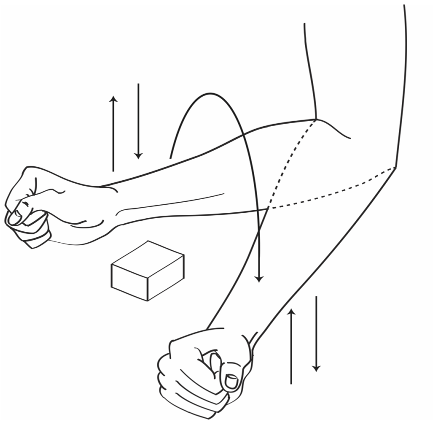

Fig. 5. Motion artifacts were generated in real-time by having the patient bump their wrist against the table on either side of a small obstacle during each contraction [38].

instructed to bump their wrist against the table once on each side of a small obstacle, pivoting on their elbow, once during each contraction, illustrated in Fig. 5. This action was intended to simulate the typical case for sEMG signal transients where the user may bump the prosthetic against an object or shift the appendage in the socket or electrode band.

To test the efficacy of the lead-off detection and handling subsystem, two Motion Tests were performed, one with mean data imputing enabled, and one without any extra processing. A single-pole double-throw continuity switch was attached to each lead pair, Fig. 4, and operated manually using a random number generator to indicate disconnect events. The generator indicated new events at a pseudo-random interval with a two second mean time interval between events and a standard deviation of one second. Disconnect events lasted for between approximately 0.2 and 0.5 seconds, and began occurring immediately after starting each test.

J. Experiment III. Simulated Real-Time

To formulate robust statistics on the effectiveness of the proposed routines, an extra set of tests were performed to see how they affected classifications for identical data sets. This was not feasible to do on live recordings, but could be done by feeding previously recorded EMG signals from Motion Tests into the microcontroller and recording the resulting classifications.

The simulated tests were performed on a data set where EMG signals were recorded from 15 able-bodied subjects performing 10 wrist and forearm movements via four bipolar electrodes placed with roughly equal spacing across the proximal third of the dominant forearm [36]. This data set was recorded at 2 kHz with a second order digital high-pass filter at 20 Hz and a notch filter centered at 50 Hz, and contained EMG data from both the pattern recognition training and the full Motion Tests. We utilized 15 Motion Tests consisting of three trials of three repetitions of each of the ten trained movements. As the EMG data for the tests were recorded using different time window parameters, only the first 128 ms in each time window, after decimating to 1 kHz, was extracted to form the training and testing sets.

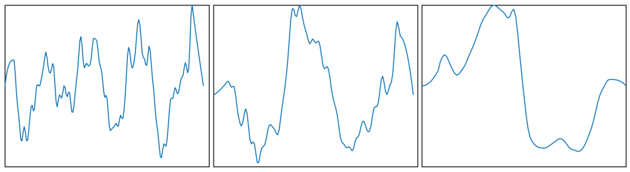

Fig. 6. Examples of transient artifact wave forms that can occur. From left to right: high-impedance, contact motion during contraction, and contact motion during rest.

The EMG data used for comparing wavelet processing with conventional filtering were modified with a set of recorded motion artifacts [12]. The artifacts, examples of which are shown in Fig. 6, were decimated and filtered to match the properties of the test EMG signal. For each time window in the Motion Test, random artifacts were added on random channels at random offsets with magnitudes corresponding to between 1 and 10 times the standard deviation of the signal strength of that window. Wavelet processing, when applicable, and pattern classification were performed on the microcontroller using a pre-trained LDA classifier by providing each time window over a serial connection and reading the resulting classifications. This test included wavelet-based artifact reduction using the third- and fourth-level transforms in addition to conventional filtering.

Noise recorded from a set of disconnected leads using the same setting as the Motion Tests was used as a data source for simulating lead-off events. The noise was then decimated to 1 kHz and separated into 128 ms time windows. Motion Test data at random time indexes on random channels on all time windows were replaced with either a random sample of recorded noise (for conventional handling) or zeros (for mean data imputing).

Neither artifacts nor lead-off events were simulated for the training data, but to compensate for the non-linear effects wavelet processing has on the data, the appropriate routine was applied to both the training and testing data for that case, illustrated in Fig. 7. The ground truth for the simulated tests in both cases was determined by running the classifier against the recorded Motion Tests without simulated LOEs or motion artifacts and saving the positions of the correct classifications. Any incorrect predictions made in this situation were ignored, as the proposed algorithms were not assumed to significantly increase the predictive power of the classifiers on clean data sets.

K. Real-Time Performance Evaluation (Experiments II-III)

A modified version of Kuiken *et al.*'s Motion Test [39] was used in each experiment to generate data for the real-time evaluation used in this work. Patients were visually cued to perform two trials of three random permutations of the movement set for each test. They were asked to hold the cued contractions at 70-80 % of maximum voluntary contraction strength until the system made 20 correct predictions or for up to 10 seconds. Signal recording, data visualization,

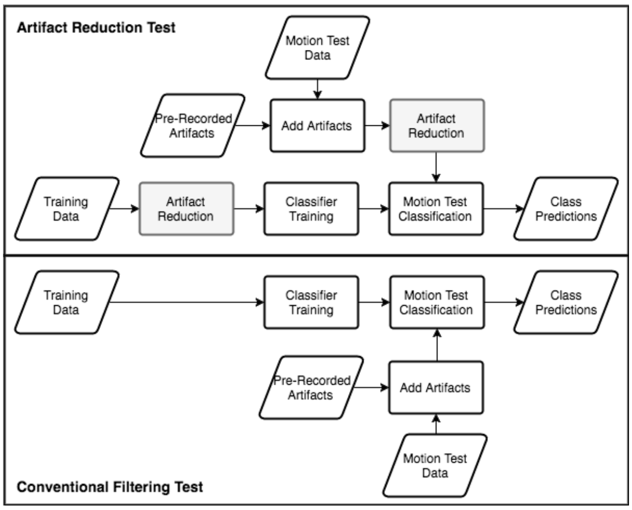

Fig. 7. Block diagram showing the training and testing procedure used to evaluate wavelet-based motion artifact reduction on pre-recorded Motion Tests

classifier training, and visual cueing were all controlled using the BioPatRec software suite running on MATLAB 2016b [36]. The mean accuracy, specificity, sensitivity, and precision across all classes were used as performance metrics for all tests in addition to completion time, selection time, and completion rate. Specificity, sensitivity, and precision metrics were included to compensate for the inherent bias of global accuracy and the disproportionately detrimental effect of false positive classifications on the controllability of prosthetic devices [40], [41].

Data imputing tests employed an additional metric referred to in this work as the *rejection rate*, defined as the percentage of class-wise false negative misclassifications resulting in no movement. This was used to show the difference in unintended movements resulting from LOEs produced by the proposed algorithm. For instance, if an LOE occurred during a close hand movement, the system would reject data from the affected electrodes, reducing the chance of interpreting an unintended open hand or wrist rotation until the electrodes regained connectivity. Two-way ANOVA tests were used on subject-specific means on each metric for statistical analysis.

Classifier training and artifact reduction on the training data were performed on a PC, and all other processing steps for the testing data, including digital filtering, wavelet-based processing, feature extraction, and pattern classification, were implemented on the microcontroller to allow for independent and mobile operation in prosthetic devices. Pattern recognition algorithms were trained using a data set recorded prior to each set of comparative tests. Embedded processing was performed on a Texas Instruments ARM Cortex-M4 processor; a full description of the hardware can be found in [37].

III. Results

A. Wavelet Parameter Selection

Motion artifact reduction with the LDA classifier without wavelet de-noising was the only set of parameters that indicated any statistically significant ($p < .05$) global accuracy improvement over conventional filtering, Fig. 8a. It also showed the smallest overall signal distortion, Fig. 8b.

B. Real-Time Test Results

Real-time test results for global classification accuracy showed no significant change between conventional filtering and wavelet-based artifact reduction, Fig. 9a Real-time data imputing tests showed a decrease in precision ($p < .01$) of 12.9 pp, but showed no other significant differences between data imputing and conventional filtering, Fig. 9b. A full summary of the results is reported in Tab. II.

C. Simulation Test Results

Simulation test results showed a statistically significant improvement ($p < .05$) in all measured metrics except selection time for both third- and fourth-level wavelet transforms, Fig. 10a. Both levels of the artifact reduction algorithm increased the selection time, indicating that the system took longer to register a movement was being attempted. The third-level wavelet processing performed best on all other metrics with an improvement in accuracy over conventional filtering ($p < .001$) by 2.0 percentage points (pp), in sensitivity by 3.1 pp, in specificity by 1.9 pp, and in precision by 6.7 pp. Data imputing showed an increase ($p < .01$) in accuracy of 4.0 pp, in specificity of 5.4 pp, and in precision of 3.5 pp, but a reduction in sensitivity of 9.2 pp, Fig. 10b. A full summary of the results is reported in Tab. II.

IV. Discussion

Phinyomark *et al.*'s work on wavelet de-noising showed significant noise reduction, but the investigation was limited to the MABS feature, leaving its effect on other signal features in question [13]. The only literature found investigating the effect of de-noising on overall classifier accuracy only showed a relatively small increase for the MLP classifier and was implemented with more neurons than considered feasible for real-time implementation in this experiment [12]. Wavelet-based de-noising may have an unseen positive effect on noise sources that more closely match real-world use, but our experiments showed it degraded performance compared to conventional filtering when presented with sEMG signals corrupted with Gaussian noise. The processing time for wavelet-based signal processing was found to increase roughly linearly with the number of active channels, which potentially limits its applicability in real-time processing on systems with a high number of channels.

The real-time experiments showed little effect from either artifact reduction or data imputing, however this was potentially a result of the testing procedure rather than due to the proposed algorithms. The motion artifacts corrupting the EMG the Motion Tests were on the order of 100 ms. With a window overlap of 64 ms, up to six windows could have been corrupted by motion artifacts from hitting the table, plus any that occurred during the transit of the forearm above the table. Given that an evaluation per movement lasts up to 10 seconds (approximately 150 time windows), the motion artifacts could

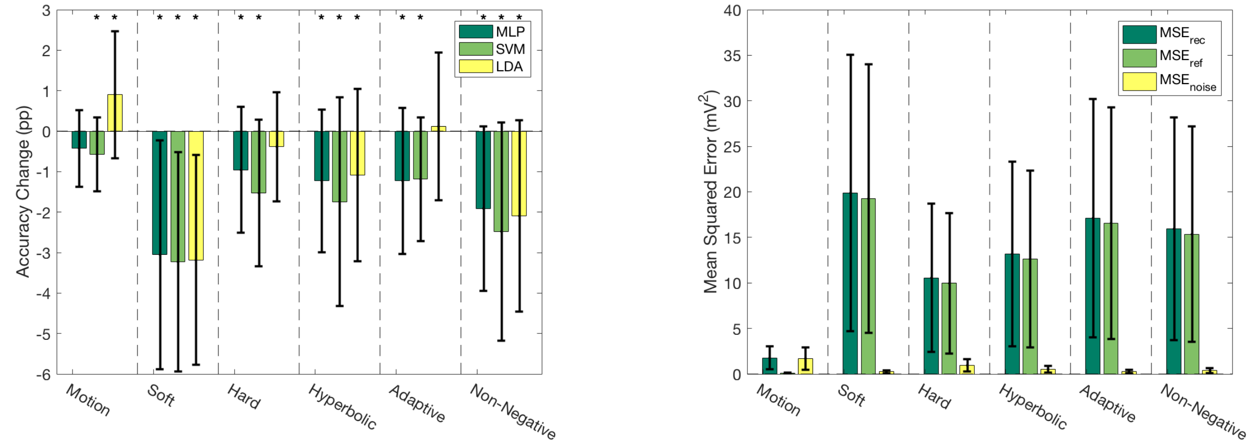

(a) Global classification accuracy change

(b) Mean squared error comparison

Fig. 8. Experiment I. Offline accuracy change and Mean Squared Error comparison of wavelet-based processing vs. conventional processing. Bars shown are mean value with indicators at ± 1 SD. Motion artifact reduction using LDA classifier showed the only significant accuracy improvement with $p < .05$

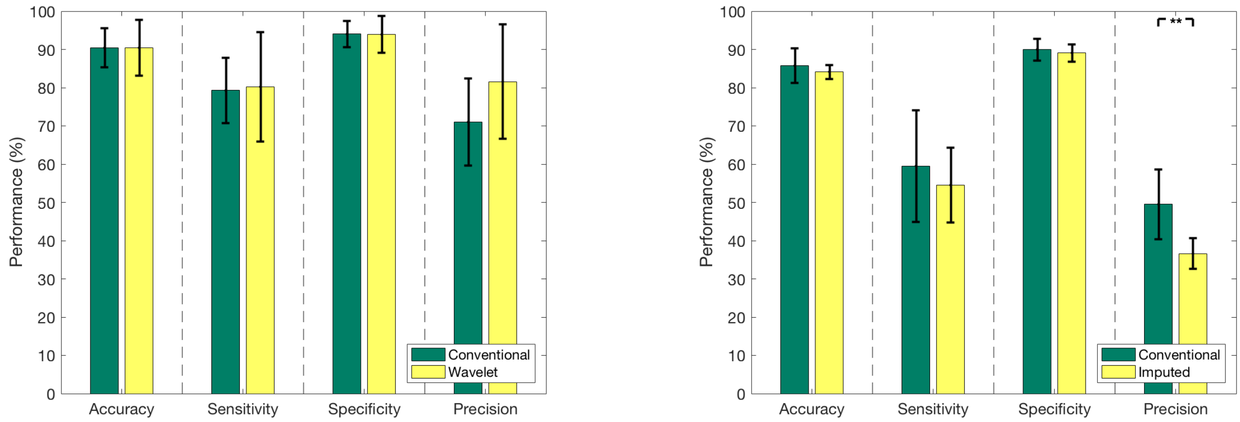

(a) Artifact reduction

(b) Data imputing

Fig. 9. Experiment II. Real-time accuracy, sensitivity, specificity, and precision metrics comparing the proposed routines with conventional signal processing. Data shown are mean values ± 1 SD. The wavelet processing algorithm used a fourth-level transform, meaning motion artifacts were assumed to have their dominant energy in the 0-31.25 Hz frequency band.

only affect a small portion of the total predictions. This was found insufficient to cause a major difference in the Motion Test outcomes, and hence the need of the simulated experiments where the signals were artificially corrupted more frequently. Similar logic applies to the small difference found when comparing conventional filtering to mean data imputing, as the lead-off events lasted between 0.2 and 0.5 seconds. In daily use and out of controlled environments, the number of episodes in which such artifacts could frustrate the user is unknown and difficult to estimate. Factors related to prosthetic fitting, such as hardware, activity level, and stump condition, would influence susceptibility to artifacts and their incidence.

The simulated experiments were expected to make more repeatable and comparable measurements than the real-time tests. Results showed a statistically significant improvement on all measured metrics, except selection time, for artifact reduction. Artifact reduction using a third-level wavelet transform showed the better performance than the fourth-level transform ($p < .001$), indicating frequency components in the motion artifacts extended past the 31.25 Hz boundary addressed by the fourth-level approximation coefficients. Clancy *et al.* suggested cable motion artifacts can extend up to around 50 Hz [42], which was corroborated by our result. Using a decreased transform order also reduces the computational complexity and memory requirements of the artifact reduction routine. Results for the simulated data imputing tests were more mixed, showing an improvement in accuracy and specificity, but with a drastically lower completion rate. These results are offset by the significant increase in the *rejection rate*, indicating that while the system completes fewer movements, the number of misclassifications resulting in unintended movements is effectively reduced. It is noteworthy to emphasize that at least

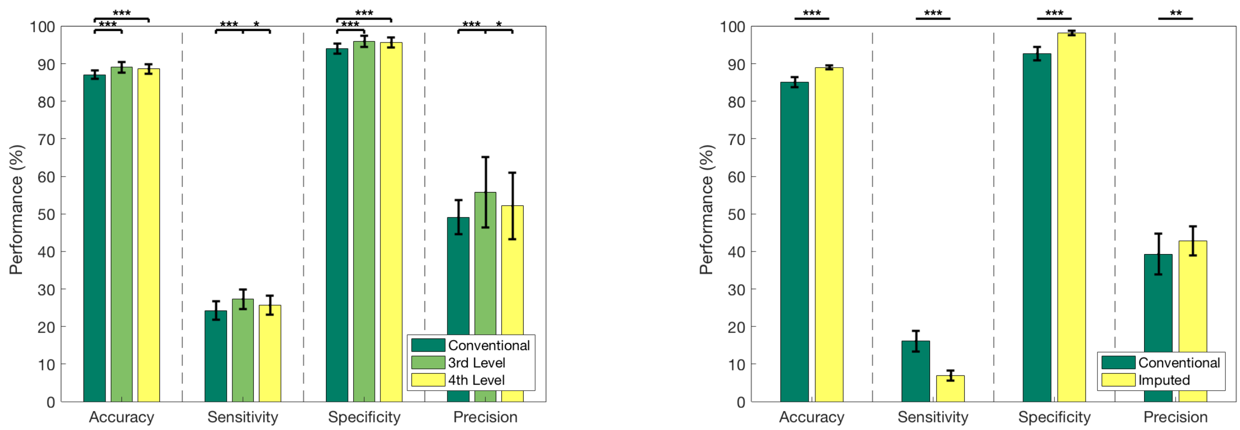

(a) Artifact reduction

(b) Data imputing

Fig. 10. Experiment III. Simulated real-time accuracy, sensitivity, specificity, and precision metrics comparing the proposed routines with conventional signal processing. Data shown are mean values ± 1 SD. Wavelet processing algorithms using both a third- and fourth-level transform were compared with conventional filtering.

TABLE II

SUMMARY OF REAL-TIME AND SIMULATED RESULTS. VALUES ARE MEANS ± 1 SD.

	Artifact Reduction			Data Imputing	
	Conventional	Third Level	Fourth Level	No Imputing	Mean Imputing
Real-Time (n=9)					
Accuracy (%)	91.7 ± 4.21		91.7 ± 5.99	87.2 ± 4.20	86.8 ± 4.88
Sensitivity (%)	79.3 ± 8.49		80.2 ± 14.3	59.5 ± 14.6	62.2 ± 13.8
Specificity (%)	94.6 ± 2.81		94.6 ± 3.99	90.9 ± 2.60	91.4 ± 3.01
Precision (%)	71.0 ± 11.4		81.6 ± 15.0	49.5 ± 9.10	36.6 ± 3.99 **
Completion Rate (%)	54.6 ± 14.0		53.7 ± 16.0	39.8 ± 9.42	38.0 ± 14.4
Selection Time (ms)	832 ± 347		898 ± 284	2000 ± 432	1750 ± 405
Completion Time (ms)	2930 ± 572		3540 ± 725 *	4210 ± 811	4170 ± 709
Rejection Rate (%)				12.7 ± 15.6	21.3 ± 19.4
Simulated (n=15)					
Accuracy (%)	87.1 ± 1.18	89.1 ± 1.40 ***	88.6 ± 1.29 ***	85.1 ± 1.38	89.0 ± 0.456 ***
Sensitivity (%)	24.2 ± 2.42	27.3 ± 2.60 ***	25.7 ± 2.54	16.1 ± 2.79	6.93 ± 1.37 ***
Specificity (%)	94.1 ± 1.35	96.0 ± 1.45 ***	95.6 ± 1.34 ***	92.7 ± 1.78	98.2 ± 0.617 ***
Precision(%)	49.1 ± 4.57	55.8 ± 9.38 ***	52.1 ± 8.86	39.3 ± 5.41	42.8 ± 3.90 **
Selection Time (ms)	243 ± 198	446 ± 210 ***	368 ± 179 *	152 ± 181	1040 ± 321 ***
Rejection Rate (%)				21.6 ± 20.2	82.0 ± 6.09 ***

(*) indicates statistical significance from null hypothesis at $p < .05$
(**) indicates statistical significance from null hypothesis at $p < .01$
(***) indicates statistical significance from null hypothesis at $p < .001$

one channel was corrupted with a lead-off event on every time window, so these results serve as a worst-case scenario, rather than a typical use-case. These results suggest that mean data imputing is an effective strategy for handling LOEs during continuous sEMG classification.

Having effective implementations of artifact reduction and data imputing on a mobile processing platform allows for more rigorous investigation into their effects on prosthetic controllability. The Assessment for Capacity of Myoelectric Control [43], the Activities Measure for Upper Limb Amputees [44], and the Southampton Hand Assessment Procedure [45] all provide advanced insight into prosthetic controllability with respect to functional tasks in real-world environments. Until now, these were infeasible for investigating wavelet-based signal processing or data imputing, due to the complexity involved with having subjects bound to a PC for processing.

V. Conclusion

In this work, we investigated the feasibility and effectiveness of implementing wavelet-based signal processing and data imputing for continuous sEMG classification on a self-contained prosthetic system. We proposed a novel and efficient method for EMG signal imputing and modifications to existing wavelet de-noising and artifact reduction routines to allow for their implementation on a wearable prosthesis. Wavelet de-noising proved ineffective for removing wide-band, Gaussian noise. Real-time tests failed to show any effect using the proposed routines, but more statistically robust simulations showed a significant improvement in classifier usability from both artifact reduction and mean data imputing. Having these systems implemented for real-time classification on a self-contained prosthesis allows for more realistic assessment, and it porentially brings pattern recognition-based prosthetic devices closer to clinical implementation.

ACKNOWLEDGMENT

The authors would like to thank the volunteers who participated in this study.

REFERENCES

[1] M. Asghari Oskoei and H. Hu, "Myoelectric control systems-A survey," *Biomedical Signal Processing and Control*, vol. 2, no. 4, pp. 275–294, 2007.

[2] B. Peerdeman, D. Boere, H. Witteveen, R. H. in 't Veld, H. Hermens, S. Stramigioli, H. Rietman, P. Veltink, and S. Misra, "Myoelectric forearm prostheses: state of the art from a user-centered perspective." *Journal of rehabilitation research and development*, vol. 48, no. 6, pp. 719–37, 2011. [Online]. Available: http://www.ncbi.nlm.nih.gov/pubmed/21938658

[3] E. Biddiss, D. Beaton, and T. Chau, "Consumer design priorities for upper limb prosthetics," *Disability and Rehabilitation: Assistive Technology*, vol. 2, no. 6, pp. 346–357, 2007.

[4] P. Gallagher, D. Desmond, and M. MacLachlan, *Psychoprosthetics*. Springer Science & Business Media, 2007.

[5] K. Østlie, I. M. Lesjø, R. J. Franklin, B. Garfelt, O. H. Skjeldal, and P. Magnus, "Prosthesis rejection in acquired major upper-limb amputees: a population-based survey," *Disability and Rehabilitation: Assistive Technology*, vol. 7, no. 4, pp. 294–303, 2012.

[6] A. Fougner, Ø. Stavdahl, P. J. Kyberd, Y. G. Losier, P. A. Parker, and S. Member, "Control of Upper Limb Prostheses : Terminology and Proportional Myoelectric Control — A Review," *IEEE Transactions on Neural Systems and Rehabilitation Engineering*, vol. 20, no. 5, pp. 663–677, 2012.

[7] D. Farina, N. Jiang, H. Rehbaum, A. Holobar, B. Graimann, H. Dietl, and O. C. Aszmann, "The extraction of neural information from the surface EMG for the control of upper-limb prostheses: Emerging avenues and challenges," *IEEE Transactions on Neural Systems and Rehabilitation Engineering*, vol. 22, no. 4, pp. 797–809, 2014.

[8] C. J. De Luca, L. D. Gilmore, M. Kuznetsov, and S. H. Roy, "Filtering the surface emg signal: Movement artifact and baseline noise contamination," *Journal of biomechanics*, vol. 43, no. 8, pp. 1573–1579, 2010.

[9] M. Reaz, M. Hussain, F. Mohd-Yasin *et al.*, "Techniques of emg signal analysis: detection, processing, classification and applications," *Biological procedures online*, vol. 8, no. 1, pp. 11–35, 2006.

[10] K. Englehart, B. Hudgin, and P. A. Parker, "A wavelet-based continuous classification scheme for multifunction myoelectric control," *IEEE Transactions on Biomedical Engineering*, vol. 48, no. 3, pp. 302–311, 2001.

[11] D. Pani, G. Barabino, S. Member, L. Citi, P. Meloni, S. Raspopovic, S. Micera, S. Member, and L. Raffo, "Real-Time Neural Signals Decoding onto Off-the-Shelf DSP Processors for Neuroprosthetic Applications," vol. 24, no. 9, pp. 993–1002, 2016.

[12] J. Maier and M. Ortiz-Catalan, "Improved prosthetic control based on myoelectric pattern recognition via wavelet-based de-noising," *Submitted to IEEE Transactions on Biomedical Circuits and Systems*, 2017.

[13] A. Phinyomark, C. Limsakul, and P. Phukpattaranont, "A comparative study of wavelet denoising for multifunction myoelectric control," in *Computer and Automation Engineering, 2009. ICCAE'09. International Conference on*. IEEE, 2009, pp. 21–25.

[14] P. Mithun, P. C. Pandey, T. Sebastian, P. Mishra, and V. K. Pandey, "A wavelet based technique for suppression of emg noise and motion artifact in ambulatory ecg," in *Engineering in Medicine and Biology Society, EMBC, 2011 Annual International Conference of the IEEE*. IEEE, 2011, pp. 7087–7090.

[15] A. Akansu, W. Serdijn, and I. Selesnick, "Wavelet transforms in signal processing: a review of emerging applications," *Physical Communication, Elsevier*, vol. 3, no. 1, pp. 1–18, 2010.

[16] P. J. García-Laencina, J.-L. Sancho-Gómez, and A. R. Figueiras-Vidal, "Pattern classification with missing data: a review," *Neural Computing and Applications*, vol. 19, no. 2, pp. 263–282, 2010.

[17] X. Zhang and H. Huang, "A real-time, practical sensor fault-tolerant module for robust EMG pattern recognition," *Journal of NeuroEngineering and Rehabilitation*, vol. 12, no. 1, p. 18, 2015. [Online]. Available: http://www.jneuroengrehab.com/content/12/1/18

[18] K. Pelckmans, J. De Brabanter, J. A. Suykens, and B. De Moor, "Handling missing values in support vector machine classifiers," *Neural Networks*, vol. 18, no. 5, pp. 684–692, 2005.

[19] G. Li, Y. Li, L. Yu, and Y. Geng, "Conditioning and sampling issues of emg signals in motion recognition of multifunctional myoelectric prostheses," *Annals of biomedical engineering*, vol. 39, no. 6, pp. 1779–1787, 2011.

[20] D. L. Donoho, I. M. Johnstone *et al.*, "Ideal denoising in an orthonormal basis chosen from a library of bases," *Comptes rendus de l'Académie des sciences. Série I, Mathématique*, vol. 319, no. 12, pp. 1317–1322, 1994.

[21] Q. Tianshu, W. Shuxun, C. Haihua, and D. Yisong, "Adaptive denoising based on wavelet thresholding method," in *Signal Processing, 2002 6th International Conference on*, vol. 1. IEEE, 2002, pp. 120–123.

[22] L. Su, G. Zhao, and R. Zhang, "Translation-invariant wavelet de-noising method with improved thresholding," in *Communications and Information Technology, 2005. ISCIT 2005. IEEE International Symposium on*, vol. 1. IEEE, 2005, pp. 619–622.

[23] B. Vidakovic, *Statistical modeling by wavelets*. John Wiley & Sons, 2009, vol. 503.

[24] H.-Y. Gao, "Wavelet shrinkage denoising using the non-negative garrote," *Journal of Computational and Graphical Statistics*, vol. 7, no. 4, pp. 469–488, 1998.

[25] C. M. Stein, "Estimation of the mean of a multivariate normal distribution," *The annals of Statistics*, pp. 1135–1151, 1981.

[26] S. P. Ghael, A. M. Sayeed, and R. G. Baraniuk, "Improved wavelet denoising via empirical wiener filtering," in *Optical Science, Engineering and Instrumentation'97*. International Society for Optics and Photonics, 1997, pp. 389–399.

[27] R. Merletti, M. Knaflitz, C. J. De Luca *et al.*, "Electrically evoked myoelectric signals," *Crit Rev Biomed Eng*, vol. 19, no. 4, pp. 293–340, 1992.

[28] A. H. plc, "Cortex microcontroller software interface standard," https://github.com/ARM-software/CMSIS_5, 2017, this work was created under the Apache-2.0 license.

[29] G. P. Nason and B. W. Silverman, "The stationary wavelet transform and some statistical applications," in *Wavelets and statistics*. Springer, 1995, pp. 281–299.

[30] M. Hakonen, H. Piitulainen, and A. Visala, "Current state of digital signal processing in myoelectric interfaces and related applications," *Biomedical Signal Processing and Control*, vol. 18, pp. 334–359, 2015.

[31] B. Hudgins, P. Parker, and R. N. Scott, "A new strategy for multifunction myoelectric control," *IEEE Transactions on Biomedical Engineering*, vol. 40, no. 1, pp. 82–94, 1993.

[32] A. Phinyomark, P. Phukpattaranont, and C. Limsakul, "Feature reduction and selection for EMG signal classification," *Expert Systems with Applications*, vol. 39, no. 8, pp. 7420–7431, 2012.

[33] M. Ortiz-Catalan, "Cardinality as a highly descriptive feature in myoelectric pattern recognition for decoding motor volition," *Frontiers in neuroscience*, vol. 9, 2015.

[34] S. Micera, J. Carpaneto, and S. Raspopovic, "Control of Hand Prostheses Using Peripheral Information," *IEEE Reviews in Biomedical Engineering*, vol. 3, pp. 48–68, 2010.

[35] I. Nabney, *NETLAB: algorithms for pattern recognition*. Springer Science & Business Media, 2002.

[36] M. Ortiz-Catalan, R. Brånemark, and B. Håkansson, "Biopatrec: A modular research platform for the control of artificial limbs based on pattern recognition algorithms," *Source code for biology and medicine*, vol. 8, no. 1, p. 11, 2013.

[37] E. Mastinu, P. Doguet, Y. Botquin, B. Håkansson, and M. Ortiz-Catalan, "Embedded system for prosthetic control using implanted neuromuscular interfaces accessed via an osseointegrated implant," *IEEE Transactions on Biomedical Circuits and Systems*, vol. PP, no. 99, pp. 1–11, 2017.

[38] J. Bowman, "Motion artifact generation illustration," 2017, this work was created under CC BY NC-SA.

[39] T. A. Kuiken, B. A. Lock, R. D. Lipschutz, L. A. Miller, K. A. Stubblefield, and K. B. Englehart, "Targeted Muscle Reinnervation for Real-time Myoelectric Control of Multifunction Artificial Arms," *Journal of the American Medical Association*, vol. 301, no. 6, pp. 619–628, 2009.

[40] M. Ortiz-Catalan, F. Rouhani, R. Brånemark, and B. Håkansson, "Offline accuracy: A potentially misleading metric in myoelectric pattern recognition for prosthetic control," in *Engineering in Medicine and Biology Society (EMBC), 2015 37th Annual International Conference of the IEEE*. IEEE, 2015, pp. 1140–1143.
[41] S. M. Wurth and L. J. Hargrove, "A real-time comparison between direct control, sequential pattern recognition control and simultaneous pattern recognition control using a fitts' law style assessment procedure," *Journal of neuroengineering and rehabilitation*, vol. 11, no. 1, p. 91, 2014.
[42] E. A. Clancy, E. L. Morin, and R. Merletti, "Sampling, noise-reduction and amplitude estimation issues in surface electromyography," *Journal of Electromyography and Kinesiology*, vol. 12, no. 1, pp. 1–16, 2002.
[43] L. M. Hermansson, A. G. Fisher, B. Bernspång, and A.-C. Eliasson, "Assessment of capacity for myoelectric control: a new rasch-built measure of prosthetic hand control," *Journal of rehabilitation medicine*, vol. 37, no. 3, pp. 166–71, 2005.
[44] L. Resnik, L. Adams, M. Borgia, J. Delikat, R. Disla, C. Ebner, and L. S. Walters, "Development and evaluation of the activities measure for upper limb amputees," *Archives of physical medicine and rehabilitation*, vol. 94, no. 3, pp. 488–494, 2013.
[45] C. M. Light, P. H. Chappell, and P. J. Kyberd, "Establishing a standardized clinical assessment tool of pathologic and prosthetic hand function: normative data, reliability, and validity," *Archives of physical medicine and rehabilitation*, vol. 83, no. 6, pp. 776–783, 2002.

Adam Naber received his B.S. degree in computer engineering from California State University, Sacramento, U.S.A. in 2013. His current research focuses on embedded systems for prosthetic control and human machine interfacing.

Enzo Mastinu received the M.Sc. degree with top grade in electronic engineering from Università degli Studi di Cagliari, Italy, in 2014. His M.Sc. thesis was awarded at the "Innovation Day Design Contest 2014," Milan, Italy. During and after the M.Sc. he was HW/FW designer for a spin-off company and a postgraduate research scholarship, respectively. He is currently working toward the Ph.D. degree at the Department of Signals and Systems, Chalmers University of Technology and Integrum AB, Gothenburg, Sweden. His research focuses on embedded systems for prosthetic control, mainly regarding upper limb amputees. Research interests cover bioelectric signal acquisition and processing, electronics design, algorithms for pattern recognition, as well as bone-anchored prostheses and osseointegration.

Max Ortiz-Catalan was born in Mexico in 1982. He received the Electronic Engineering degree from the ITESM Campus Toluca, Mexico, in 2005, the M.Sc. degree in complex adaptive systems, and the Ph.D. degree in biomedical engineering from Chalmers University of Technology (CTH), Gothenburg, Sweden, in 2009 and 2014, respectively. He is currently an Assistant Professor at CTH, where he founded the Biomechatronics and Neurorehabilitation Laboratory (@ChalmersBNL). He works in close collaboration with the Centre for Advanced Reconstruction of Extremities (C.A.R.E.) at Sahlgrenska University Hospital, Gothenburg, Sweden. He also serves as the Research Director for Integrum AB, Gothenburg, Sweden. His research interests include bioelectric signals acquisition electronics (analog and digital); signal processing and artificial intelligence algorithms for pattern recognition and control; neuromuscular interfaces; bone-anchored prostheses and osseointegration; as well as virtual and augmented reality for neuromuscular rehabilitation and the treatment of phantom limb pain. He received the "You Can Make a Difference Award" in 2006, the "European Youth Award" in 2014, the "Delsys Prize" in 2016, and the "Brian & Joyce Blatchford Award" in 2017.